Aggregation of Amphiphilic Molecules in Solution: Thermodynamics, Metastability, and Kinetics

Thesis submitted for the degree of

Doctor of Philosophy

by

Radina Hadgiivanova

Submitted to the senate of Tel Aviv Univeristy

October 2009

This work was carried out under the supervision of

Prof. Haim Diamant

Acknowledgements

I would like to express deepest gratitude to my supervisor Prof. Haim Diamant. His continuous support made completing my PhD possible. I have benefited greatly from his willingness to help with any problem I had, not only in science but also in personal matters. I have been constantly inspired by his deep knowledge and understanding of physics and his perfectionism. I would like to thank him for always keeping his door open for me. I could not have dreamed of a better supervisor.

I would also like to thank Prof. Ralf Metzler from the Technical University of Munich for his hospitality and kindness. The help and advice I received during my stay in his group were of great benefit to me.

I am indebted to Prof. David Andelman for the collaboration and helpful comments to Chapter 4 of this thesis.

I want to express my gratitude to Prof. Shmuel Carmeli and Yehudid Lev thanks to whom I have received financial support during the last two years of my PhD studies.

I thank my colleague Emir Haleva for all the help and good advice. I'm very grateful for his great friendship.

Last, but not least I would like to thank my parents, and especially my mother, for supporting me financially and morally during my studies.

Abstract

Amphiphiles are molecules, which have covalently bonded hydrophilic (soluble in water) and hydrophobic (insoluble in water) groups. In aqueous solution such molecules self-assemble into aggregates of various shapes and sizes. Many amphiphiles (*e.g.*, surfactants, block copolymers) form spherical aggregates called micelles above a certain amphiphile concentration, known as the *critical micelle concentration* (cmc).

This thesis addresses current issues in the theory of micellar aggregation and aims to give a unified theoretical description of some of the "universal" features of micellar solutions.

Throughout this work we use a simple free-energy formalism, which views micellization as restricted nucleation. That is, the micelles are treated as nuclei of an aggregated phase, with the difference between micellization and macroscopic phase transition being the finite size of the micelles. Despite its simplicity our model enables us to study a host of new issues related to amphiphilic aggregation in and out of equilibrium.

The first issue we address is the phenomenon of premicellar aggregation (*i.e.*, the possible appearance of micelles below the cmc). This phenomenon and its features have been a subject of dispute among scholars during the years. Sensitive spectroscopic techniques like FCS, as well as NMR measurements, show in some cases the appearance of micelles at concentrations as low as 3-4 times below the literature known value of the cmc (as measured by macroscopic techniques such as conductivity and surface tension). This effect has often been attributed to the presence of a third component in the system (eg., a fluorescent dye), which participates in the formation of micelles and therefore lowers the cmc. We propose a different explanation. We study micellar aggregation using our free-energy model. It accounts for metastable states in the system, which we identify as premicellar aggregates. We examine the characteristics of these premicellar aggregates (aggregate size, polydisperisity, kinetic stability). We find that, for certain realistic values of parameters and assuming strict equilibrium, there should be an

appreciable extent of premicellar aggregation below the cmc. There is, however, a high free energy barrier for the nucleation of such metastable aggregates. Thus, the impurities (e.g., dyes) introduced in various experiments may act as nucleation centers, which facilitate the kinetics rather than shift the cmc.

The second part of the thesis regards the kinetics of nucleation and growth of the spherical micelles in different experimentally relevant scenarios (*e.g.*, a concentration jump). Previous theories model this problem as a step-wise chemical reaction and contain a large number of free parameters. In this thesis we present a new approach to the study of micellization kinetics, which is easily tractable and generalizable. We derive kinetic equations, which describe the kinetics as various pathways along the free-energy landscape. The kinetics of micelle formation and growth is examined in two different scenarios, namely an open system connected to a reservoir at amphiphile concentration above the cmc, and a closed system which undergoes a concentration quench. The kinetics of the two scenarios are shown to be strikingly different. In both cases separation of time scales is found, leading to distinct stages in the kinetics (nucleation, growth and final relaxation). Our results are in qualitative agreement with experimental evidence whenever such exists.

The thesis demonstrates the power and generality of our free-energy formalism, which can be extended to further studies of amphiphilic aggregation in the future.

Contents

Chapter 1

General Introduction

This chapter gives a brief overview of the amphiphilic self-assembly phenomena in general and of the theoretical and experimental research of micellization done in the past. It also reviews the theoretical methods to be used in the next chapters of this thesis.

Section 1.1 deals with the driving force of amphiphilic self-assembly. Section 1.2 describes the characteristics of the phenomenon. Sections 1.3 and 1.4 give a brief review of the study of micellar aggregation. Sections 1.5 and 1.6 provide some theoretical background for the following chapters, and Section 1.7 presents the contents of this thesis.

1.1 The hydrophobic effect

The driving force for amphiphilic self-assembling systems is the so-called hydrophobic effect. The term hydrophobic effect [1] was coined by Charles Tanford in the 1970s to explain the tendency of non-polar molecules to form aggregates of like molecules in water. A full understanding of this phenomenon is still lacking because of the many intermolecular interactions involved. It is known, however, that the main reason is entropic and is due to the unique properties of the water molecules. When a non-polar molecule is placed in water, the water molecules around it have to create a cavity to accommodate it. Since non-polar molecules cannot form hydrogen bonds the creation of the cavity requires either breakage of hydrogen bonds, or rearrangement

of the water molecules in a way that breaking of hydrogen bonds is avoided. Which process takes place depends of course on the details of the solute molecule. The tetrahedral shape of the water molecules allows them to arrange themselves around most solutes without breaking hydrogen bonds but in this process the water molecules become even more ordered than in bulk water, which is entropically unfavorable. This is the reason why inert substances like hydrocarbons are immiscible in water. When many such molecules are present in water the loss of entropy becomes too great and it becomes more favorable to break hydrogen bonds and create larger cavities to accommodate an assembly of non-polar molecules, *i.e.*, to form aggregates of solute molecules. This leads to an effective attraction between the non-polar molecules, called the hydrophobic interaction. Due to the hydrophobic interaction, the non-polar molecules have stronger mutual attraction in water than they do in free space.

The hydrophobic effect is very important in nature. It is the reason for the formation of lipid membranes and affects many other biological processes, *e.g.*, protein folding. In soft matter it plays a role in many systems, in particular, it is the driving force for amphiphilic self-assembly.

1.2 Amphiphilic self–assembly

Amphiphile is a general term that describes any molecule that has covalently bonded hydrophilic and hydrophobic parts. Examples of amphiphiles are surfactants, block copolymers, lipids, bile acids, cholesterol and many other [2, 3, 4]. In water, due to the hydrophobic effect, amphiphiles form a variety of structures (assemblies), which minimize the contact between the hydrophobic part of the amphiphile and the water molecules, while optimizing the repulsion between the hydrophilic head-groups. The type of assembly depends on the amphiphile's structure, its concentration, temperature and pressure [2]. At very low concentration the amphiphile forms a monolayer at the water-air interface. Above a certain concentration, called the critical aggregation concentration (cac), it self-assembles into different structures *e.g.*, rods, discs, spheres, bilayers and vesicles. At concentrations much higher than the cac, amphiphiles may form diverse liquid-crystalline phases, *e.g.*, bilayer stacks (lamellar phase) and hexagonal phases [2, 3, 4, 5].

To predict the size and shape of the structures for a given set of conditions (*e.g.*, temperature, pH, concentration) simple theoretical models (*e.g.*, [2, 6]) look at amphiphilic self-assembly as a process governed by two "opposing forces" [1], acting mainly at the interface between the surfactants and water. The attractive interaction between the monomers is due to the hydrophobic effect (Sec. 1.1), which makes the molecules associate, and the repulsive interaction is due to electrostatic or steric repulsion between the hydrophilic head groups and requires that the head groups stay in contact with water. Thus, a balance is achieved at a certain interfacial area, a_0, per molecule exposed to the aqueous phase. Once the volume, v, of the hydrophobic portion of the molecule and its length, l_c, are known, the type of assembly can be deduced by geometric packing considerations. It depends on the packing parameter $\frac{v}{a_0 l_c}$ as shown in Fig. 1.1.

The simplest type of amphiphiles are surfactants which have one hydrocarbon chain, containing between 8 and 18 carbon atoms, for a hydrophobic part. They are classified according to the type of hydrophilic head group as ionic, zwitterionic and non-ionic. Above a certain concentration, called the critical micellar concentration (cmc), these amphiphiles form spherical aggregates called micelles. Due to their simplicity relative to other self-organizing systems, micelles are often used as a model system for the study of self-assembly. Another reason for the interest in them are the many technological applications of micellar solutions.

The applications of micelles in many fields of science and technology are numerous [4, 7, 8]. In colloid chemistry spherical micelles are used as a model system for studying many problems, for example the various interactions between colloid particles. In biology they are a good system for the study of the factors involved in the hydrophobic effect. There are biological systems, such as the bile, that directly involve micelles. In chemistry micelles are used as catalysts and solubilizing agents in many organic and inorganic reactions. In industry and technology most of the applications of micelles are based on their ability to solubilize. They are used in cleansing as detergents, in medicine for encapsulating drugs in their hydrocarbon cores, in oil recovery for solubilizing oil droplets. Inverted micelles in non-aqueous media are used in motor oils to solubilize oxidizing agents and thus prevent them from reacting with engine parts [9]. Many biological and technological processes are strongly influenced by the rate

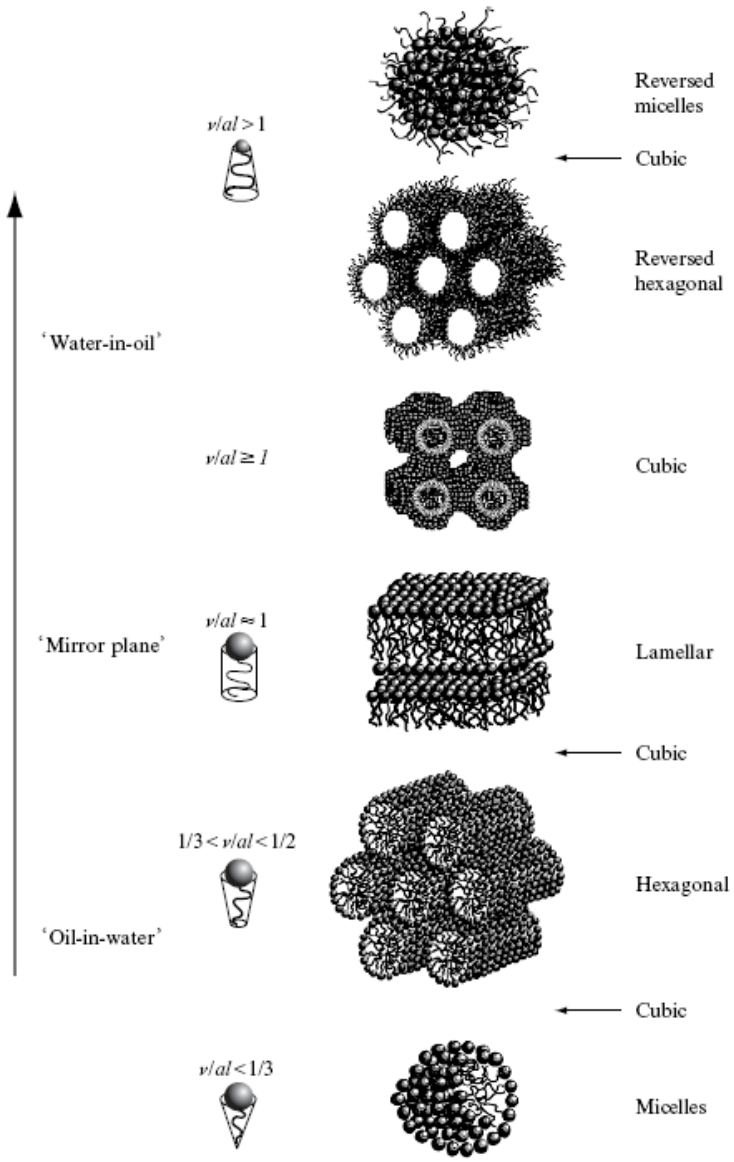

Figure 1.1: Dependence of aggregate morphology on the packing parameter (from Ref. [4]).

of micelle formation and growth, *e.g.*, foaming and stabilization of microemulsions. Apart from solubilization, there is the key role of surfactants in reducing surface tension (e.g., in wetting and coating processes).

The understanding of self-assembly in general, the invention of new applications of micellar solutions in technology and science, and the improvement of the existing ones, require theoretical understanding of the system. It is one of the reasons why the theoretical and experimental study of micellization has been done extensively in the past. Many aspects of the system are not yet fully understood and are a subject of debate. More is known about the thermodynamic characteristics of micellar solutions.

The possible metastability of micellar solutions and the kinetics of micelle formation and growth, on the other hand, are much less studied and further research in that direction is needed.

1.3 Thermodynamics of micellar aggregation

1.3.1 Experimental observations

The critical micellar concentration (cmc)

Experimentally the cmc is measured by many microscopic and macroscopic techniques. The most common methods are conductivity (for ionic surfactants) and surface tension. Many other techniques are employed as well. Some examples are shown in Fig. 1.2. The cmc is usually determined as the point of intersection of two lines that interpolate the experimental data for low and high surfactant concentrations. Other definitions are used as well [10]. For example, the cmc is sometimes determined as the point of maximum curvature of the plotted macroscopic property of the micellar solution (*e.g.*, conductivity, or surface tension) as a function of surfactant concentration.

The cmc depends on the chemical structure of the surfactant and many external factors, *e.g.*, pH, temperature and pressure [4, 11]. For example, it decreases strongly with increasing the hydrocarbon chain length of the surfactant. This is because the critical chemical potential, $k_{\mathrm{B}}T\log(\mathrm{cmc})$, decreases linearly with chain length, with each methyl group contributing about 2-3 $k_{\mathrm{B}}T$. The cmc of ionic surfactants (typically $10^{-3}-10^{-2}$M) is orders of magnitude higher than the one of nonionic amphiphiles (typically $10^{-5}-10^{-4}$M). This is due to the smaller repulsion between the headgroups in the nonionic case. The addition of salt decreases the cmc of ionic surfactants by up to an order of magnitude. This effect is due to the electrostatic screening caused by the salt ions, which reduces the repulsion between the ionic head groups. The cmc of non-ionics is slightly affected by salt addition, which can go in both directions (decrease or increase).

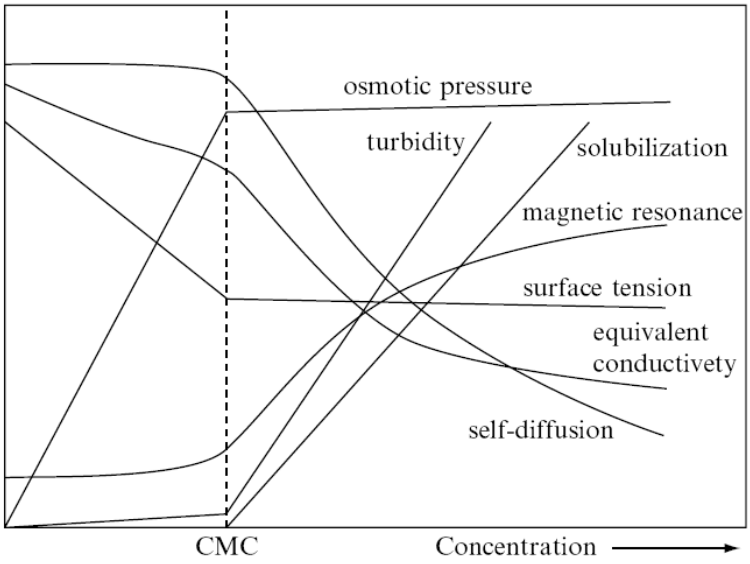

Figure 1.2: Schematic representation of the concentration dependence of some physical properties of micelle-forming surfactant solutions (From Ref. [9]).

The micelle size

The micelle size is characterized either by the radius of the micelle, or the number of monomers in a micelle, called the micelle aggregation number. These can be measured by light scattering and fluorescence quenching techniques [4, 11]. Typical values for the aggregation number are between 10 and 100. Surfactants with longer hydrocarbon chain length are known to form larger micelles. The spherical micelles have small polydispersity, which allows one to assume that they are monodisperse, thus simplifying the theoretical modeling of the system. One can also assume that the surfactant volume is conserved in the process of micelle formation, thus considering the micellar core as an incompressible oily "droplet".. The same factors that affect the cmc affect the micelle size as well. For example, the addition of electrolyte leads to the formation of larger micelles for the ionic surfactants due to screening of inter-molecular repulsion.

1.3.2 Thermodynamic models of micellization

Since amphiphilic self-assembly involves structures of finite yet large size (micelles containing tens to hundreds of molecules), a rigorous statistical-mechanical treatment of the interactions in such a system is a formidable task. Consequently, analytical models have resorted to phenomenological approaches, trying to account for the various

competing interactions while assuming a certain aggregate geometry [2], [6]–[16]. Of these, the prevalent model of micellization has been that of Israelachvili, Mitchell, and Ninham [2, 6], in which the cmc and aggregate shape and size are derived from thermodynamic analysis and simple geometrical arguments related to molecular packing. (See the discussion in Sec. 1.2 and Fig. 1.1.) The system is modeled using mass-action considerations. That is, analogy is drawn between micellization and chemical equilibrium among reactants. Aggregates of different sizes are treated as distinct chemical species. From this model the fraction of molecules in aggregates of size m (*i.e.*, made of m molecules), x_m, is given by,

$$x_m = m\{x_1 \exp[\mu_1^0 - \mu_m^0]\}^m, \tag{1.1}$$

where μ_m^0 is the standard part of the chemical potential (in units of $k_{\rm B}T$) of a molecule in an aggregate of size m. For a compact (spherical) micelle, which is treated as a "droplet", μ_m^0 is related to a surface-energy penalty and, therefore, is inversely proportional to the radius of the "droplet" (area divided by m). Thus,

$$x_m = m\{x_1 \exp[u(1 - 1/m^{1/3})]\}^m \approx m[x_1 e^u]^m, \tag{1.2}$$

where u is the monomer-monomer "bond" energy in units of $k_{\rm B}T$ in the aggregate relative to isolated monomers in solution. Since $x_m \leq 1$ the maximum value that x_1 can reach is $x_1 \approx e^{-u}$. This value is inferred as the cmc in the model. Therefore, so long as $x_1 < e^{-u}$, any increase in the concentration increases the number of monomers, whereas for $x_1 > e^{-u}$, the fraction of monomers remains essentially fixed at the cmc and additional molecules form micelles.

More detailed theories have been proposed in the past few decades, attempting to phenomenologically account for various molecular effects involved in micellization [14]–[17], or take into account the detailed configurational statistics of the hydrocarbon tails (e.g., [18]–[20]). A host of computer models for amphiphilic self-assembly have been presented as well (e.g., [17], [21]–[25]).

1.4 Micellar kinetics

1.4.1 Experiments

Dynamic aspects of micellar aggregation have been extensively studied in the past as well [11]. The efforts in this field were most numerous in the 1970s, when some kinetic properties, like dissociation/association rates became accessible. They can be measured by techniques like temperature-jump, pressure-jump, stopped flow (concentration-jump), ultrasonic absorption, NMR and ESR. The first three methods study the relaxation process of a system, which is driven out of equilibrium by a sudden perturbation. The last two methods measure the spectral change caused by the change in the monomer exchange rate between an aggregate and the bulk. These techniques and the interpretation of their results have used the framework of first-order reaction kinetics, where each aggregate size is treated as a distinct chemical species, and changes in size and population — as chemical reactions (Chapter 3 of Ref. [11]). Two well separated time scales are identified in the experiments [26]. The shorter of the two (typically $\sim 10^{-6}$–10^{-4} s) corresponds to the exchange of a single molecule between a micelle and the monomeric solution; during this time scale the number of micelles remains essentially fixed. The second (*e.g.*, $\sim 10^{-2}$ s) is associated with overcoming the barrier to the formation or disintegration of an entire micelle; during this longer time scale the number of aggregates changes.

1.4.2 Theoretical models

A theoretical explanation of the relaxation experiments was first proposed by Aniansson and Wall [27] and is still the prevalent theory of micellar kinetics. They model the micellar association/dissociation as a series of step-wise chemical reactions, where at each step only one monomer enters or leaves an aggregate of size m, A_m,

$$A_1 + A_{m-1} \underset{k_m^-}{\overset{k_m^+}{\rightleftharpoons}} A_m, \quad m = 2, 3, 4, ... \tag{1.3}$$

k_m^+ and k_m^- are the forward and reverse rate constants for the $(m-1)$th step, respectively. One of the assumptions made in the theory is that in the solution there are only free monomers and aggregates with Gaussian-distributed size with average $\langle m \rangle$

and variance σ^2. That is, there is a negligible amount of aggregates of intermediate size $1 < m < m - \sigma$. Therefore, after the system is perturbed the size and number of aggregates will adjust themselves to the new equilibrium state by a quasi-steady-state process, where the rate limiting step is the passage through the intermediate aggregate size. The following equation for the fast relaxation time, τ_1, is derived

$$\frac{1}{\tau_1} = \frac{k^-}{\sigma^2}\left(1 + \frac{\chi\sigma^2}{\langle m\rangle}\right), \tag{1.4}$$

with $\chi = (C - \mathrm{cmc})/\mathrm{cmc}$ and k^-, the m-independent dissociation rate constant in the region of the micelles, $m = \langle m\rangle \pm \sigma$. The last equation predicts a linear dependence of $1/\tau_1$ on the total surfactant concentration, C, which is in agreement with experiments. Under the same assumptions the slow relaxation time, τ_2, is found to satisfy,

$$\frac{1}{\tau_2} = \frac{\langle m\rangle^2}{\mathrm{cmc}R}\left(1 + \frac{\chi\sigma^2}{\langle m\rangle}\right)^{-1}, \tag{1.5}$$

where

$$R = \sum_{m=2}^{\langle m\rangle-\sigma} \frac{1}{k_m^- A_m}. \tag{1.6}$$

Here R is viewed as the resistance to flow through the region of intermediate sized micelles. The dependence of $1/\tau_2$ on concentration, temperature and other factors is determined by their effect on R. One can also calculate the mean lifetime of a micelle, τ_m, [28]

$$\tau_m = \tau_2 \frac{\langle m\rangle\chi}{\left(1 + \frac{\chi\sigma^2}{\langle m\rangle}\right)}. \tag{1.7}$$

For concentrations significantly higher than the cmc it is approximately equal to $\langle m\rangle\tau_2$.

More detailed models [30], based on the same scheme, include electrostatic effects for ionic surfactants and the possibility of fusion/fission of two micelles. While various extensions to the Aniansson-Wall theory have been presented over the years [28]–[36], only a few alternative approaches have been suggested. In Ref. [37] the interesting possibility that micellization may behave as a bistable autocatalytic reaction was explored. An idealized nucleation model for linear aggregates was suggested in Ref. [38].

In the case of micellization of amphiphilic block copolymers more progress has been

achieved (Chapter 4 of Ref. [11]; [39]–[46]). The kinetics of such polymeric micelles, however, usually depend on qualitatively different effects, in particular, the high entropy barrier for polymer penetration into a micelle. The kinetics of micellization was studied also by computer simulations (*e.g.*, Refs. [47, 48]).

The following sections of this chapter give some theoretical background for the methods used in the next chapters of this thesis. As mentioned in the abstract micellization is treated as a process of restricted nucleation and, therefore, the methods used in the study of phase transitions will be summarized. Since the micelles are much larger than molecular size one needs to use an appropriate model for the calculation of the entropy of mixing of such species.

1.5 Entropy of mixing

The entropy of mixing of two species, A and B, which have different molecular size is typically calculated using a lattice model [49]. The lattice cell volume, a^3, is taken as the smallest relevant volume in the system (for example, the volume of a solvent molecule or a monomer in a polymer chain), and larger molecules occupy multiple connected sites. It is assumed that there is no volume change upon mixing. The volume fraction of species A will therefore be $\phi_A = V_A/(V_A + V_B)$ and that of species B, $\phi_B = V_B/(V_A + V_B) = 1 - \phi_A$. A molecule of species A has a volume, $v_A = n_A a^3$, and that of species B has a volume $v_B = n_B a^3$, where n_A and n_B are the number of lattice sites occupied by species A and B, respectively. The total volume of the system is $V = V_A + V_B$, and the total number of lattice sites is $N = V/a^3$. The entropy, S of the system is determined by $S = k_\mathrm{B} \ln \Omega$, where k_B is the Boltzmann constant and Ω the number of states—here the number of different translational configurations on the lattice.

The number of states of a molecule of species A before mixing, Ω_A, is equal to the number of lattice sites occupied by species A, *i.e.*, $\Omega_A = N\phi_A$. Therefore, the change of entropy per molecule of species A upon mixing is

$$\Delta S_A = k_\mathrm{B} \ln \Omega - k_\mathrm{B} \ln \Omega_A = -k_\mathrm{B} \ln \phi_A. \tag{1.8}$$

Since $\phi_A < 1$, the change of entropy upon mixing is always positive. By the same argument the change of entropy per molecule on mixing of species B is $\Delta S_B = -k_\mathrm{B} \ln \phi_B$. This gives for the total entropy of mixing,

$$\Delta S_{mix} = N_A \Delta S_A + N_B \Delta S_B = -k_\mathrm{B}(N_A \ln \phi_A + N_B \ln \phi_B), \tag{1.9}$$

where $N_A = N\phi_A/n_A$ and $N_B = N\phi_B/n_B$ are the number of molecules of species A and B, respectively. We can define the entropy of mixing per lattice site, $\Delta \bar{S}_{mix} = \Delta S_{mix}/N$, which is an intensive thermodynamic quantity.

For a regular solution, made of two molecular species of similar size, say, $n_A = n_B = 1$, the entropy of mixing is larger than the one of a solution, where the solute is a large molecule, *e.g.*, polymer or colloid and the solvent molecular, $n_A = n$ and $n_B = 1$. In the latter case the entropy of mixing could be a lot smaller if n is large.

Let $\phi_A = \phi$ be the volume fraction of the solute ($n_A = n$) and $\phi_B = 1 - \phi$ the volume fraction of the solvent ($n_B = 1$) in a binary solution. Then the free energy of mixing per lattice site of an ideal mixture is

$$\Delta \bar{F}_{mix} = -T\Delta \bar{S}_{mix} = k_\mathrm{B}T \left[\frac{\phi}{n} \ln \phi + (1-\phi) \ln(1-\phi) \right]. \tag{1.10}$$

In a similar way the entropy and free energy of mixing for multicomponent ideal mixtures can be calculated. It is given by

$$\Delta \bar{F}_{mix} = k_\mathrm{B}T \sum_i \frac{\phi_i}{n_i} \ln \phi_i, \tag{1.11}$$

where ϕ_i and n_i are the volume fraction and number of lattice sites occupied by a molecule of species i, respectively.

As mentioned earlier, in the next chapters of this thesis the framework of first-order phase transitions will be used to study micellization. Therefore, a short overview on this subject follows.

1.6 First-order phase transitions

The transition of a system from one phase to another, *e.g.*, vapor to liquid, ordered to disordered phase, on changing some parameter of the system, *e.g.*, temperature, pressure, concentration of a component, is a vast field of study [50, 51, 52]. The transition occurs at a critical value of a control parameter of the system, *e.g.*, temperature. Phase transitions are classified by the lowest derivative of the free energy that is discontinuous at the transition. First-order phase transitions exhibit a discontinuity in the first derivative of the free energy with respect to a thermodynamic variable. For example, a gas–liquid transition is classified as first-order transition because it involves a non-analytic change in density (which is the first derivative of the free energy with respect to chemical potential.) Second-order phase transitions are continuous in the first derivative but exhibit discontinuity in a second derivative of the free energy. Here we shall concentrate on first-order phase transitions because the framework will serve as a basis for the models to be described in Chapters 2, 3 and 4.

When a system undergoes a first-order phase transition, the dynamics can proceed in two main pathways—nucleation and growth, or spinodal decomposition. The pathway depends on the depth of the quench that the system has undergone, *i.e.*, how far from its critical value the control parameter has been set. If the quench is sufficiently deep, leading to the formation of an unstable state, *i.e.*, the free energy has only one minimum, at a new equilibrium state, the phase separation will proceed via spinodal decomposition. This process requires an arbitrarily small fluctuation of the order parameter to form the new phase. If, however, the quench brings the system into a metastable state, an energy barrier has to be overcome to reach the new equilibrium stable state. The process of overcoming an energy barrier requires the occurrence of larger fluctuations in the order parameter and the phase transition proceeds via nucleation.

1.6.1 Nucleation

The nucleation process can be simply described using the so-called "droplet model" [52]. The phase transition starts with formation of small nuclei of the new phase, which then grow or disappear depending on their size. It is assumed that these nuclei

are spherical in shape and the free energy difference, ΔG, of the formation of a nucleus with radius R, has two competing terms, which determine whether the formation of the nucleus is energetically favorable,

$$\Delta G = \frac{4}{3}\pi R^3 \Delta\mu + 4\pi R^2 \gamma. \tag{1.12}$$

The first term is proportional to the volume of the droplet and the difference in chemical potential, $\Delta\mu$, of a molecule that changes phase and joins the droplet. It is always negative, *i.e.*, favors the formation of the droplet since the system is in a metastable state ($\Delta\mu < 0$). The second term is proportional to the area of the nucleus and the surface tension coefficient, γ, between the two phases. It is positive since the formation of an interface between the phases is energetically unfavorable. The competition of these two terms leads to the existence of a free-energy nucleation barrier, ΔG^*, at a critical nucleus radius, R^*. These are obtained from $\left(\frac{\partial \Delta G}{\partial R}\right)_{R=R^*} = 0$, yielding

$$R^* = -\frac{2\gamma}{\Delta\mu}, \qquad G^* = \frac{16\pi}{3}\frac{\gamma^3}{\Delta\mu^2}. \tag{1.13}$$

Thus, if due to fluctuations of the order parameter a droplet with radius larger than R^* is formed, it will continue to grow until it reaches macroscopic size. If the radius is smaller than R^*, it will dissociate. In Chapter 2.1, we will use a similar picture to model the free energy of transfer of a free monomer into a micelle.

1.6.2 Steady-state nucleation rate

The rate at which new nuclei form was to first approximation estimated as proportional to the exponential of the nucleation barrier, by analogy with the Arrhenius law in chemical kinetics and the activation energy barrier. One of the first theories to treat the problem in a more rigorous way, and give an estimate of the pre-exponential factor, was due to Becker and Döring [53]. Later theories, based on the same formalism, tried to improve the prefactor, referred to as the Zeldovich factor, using different phenomenological expressions and taking into account heterogeneous nucleation [54].

A theory which solves the basic problem of escape of a diffusing particle from a

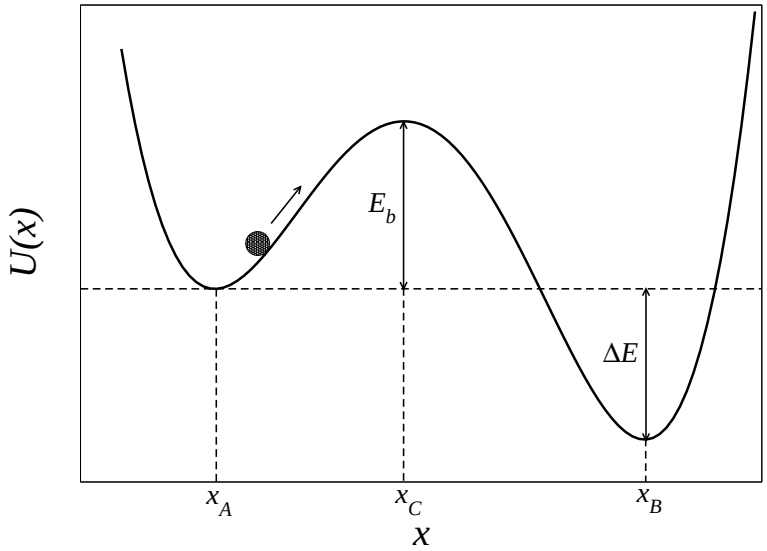

Figure 1.3: Double well potential $U(x)$ with minima at x_A and x_B and maximum at x_C. The particle has to overcome the energy barrier E_B to reach its stable state at x_B.

potential well and is applicable to the calculation of nucleation rates, is Kramers' theory [54, 55]. It has many similarities with the Becker–Döring theory but contains fewer fitting parameters and can be used to calculate the escape rate for any type of potential. The escape of a particle from a metastable to a stable state over an energy barrier is shown in Fig. 1.3. Kramers' theory assumes that the energy barrier, E_b, is larger than $\sim 10k_{\mathrm{B}}T$ and that the energy difference, ΔE, between the initial and final states is sufficiently large. The first condition leads to separation of time scales and allows one to assume that steady-state is achieved. The second condition ensures that there will be a negligible flux of particles from the final back to the initial well. The following expression for the escape rate, τ^{-1}, is found,

$$\tau^{-1} = \frac{D}{4\pi}\omega(x_A)\omega(x_C)e^{-E_b}, \tag{1.14}$$

where D is the diffusion coefficient of the particle, $\omega(x_A) = [U''(x_A)]^{1/2}$ and $\omega(x_C) = [U''(x_C)]^{1/2}$, are the width of the well at x_A and the width of the maximum at x_C, respectively, and $E_b = U(x_C) - U(x_A)$ is the energy barrier (in units of $k_{\mathrm{B}}T$). There-

fore, the escape rate is exponentially proportional to the energy barrier, analogous to Arrhenius law, but it also depends on the characteristics of the potential through the pre-exponential factor.

1.6.3 Spinodal decomposition

For a system quenched into the unstable spinodal region, the phase transition does not involve climbing over free-energy barriers and the process is purely dissipative. So long as we are not too far from equilibrium, the change of the order parameter, ξ, with time can be related to the variation of the free energy functional, $F[\xi]$, with respect to the order parameter. There are two types of dynamics corresponding to different types of order parameters. If the order parameter is a non-conserved quantity, *e.g.*, magnetization, the dynamics can be described by an equation of the form

$$\frac{d\xi}{dt} = -\Gamma \frac{\delta F}{\delta \xi}. \tag{1.15}$$

Here Γ is a response coefficient. Such a scheme leads, e.g., to the Allen-Cahn equation [52]. This is a deterministic equation derived from the Langevin equation under the assumption that the coarse-grained free energy functional has a mean-field Landau-Ginzburg form and neglecting the random noise term. For locally conserved order-parameter, *e.g.*, particle concentration, one has to include conservation laws. Usually the particle flux is assumed proportional to the gradient of the local chemical potential difference. This leads to the Cahn-Hilliard equation [51].

In Chapter 4 we will make use of equations similar to Eq. 1.15 to study stages of micelle growth after a nucleation stage.

1.6.4 Coarsening

In the late stages of phase separation, the droplets of the new phase undergo a process of coarsening known as Ostwald ripening [52]. Since larger droplets are more energetically stable (due to their smaller interfacial area-to-volume ratio) than smaller droplets, they tend to grow on the expense of the smaller ones. This process is diffusion controlled, *i.e.*, the rate at which the bigger droplets grow depends on the diffusion

rate of monomers leaving the smaller droplets and diffusing toward the bigger ones.

In micellar solutions, where the equilibrium size of the aggregates is finite, the positive-feedback mechanism underlying Ostwald ripening is absent. One can then imagine different types of coarsening processes, for example, fusion of two micelles to form a larger one, or fission of one micelle into two smaller aggregates. Computer simulation studies, *e.g.*, [24], observe these phenomena under certain conditions.

1.7 Thesis overview

To conclude this introductory chapter we briefly describe the thesis structure. The work is based on a free-energy formalism which is presented in Chapter 2. In the following Chapters, 3 and 4, we develop various applications of the formalism. The first application is for the study of premicellar aggregation, which is presented in Chapter 3. In Chapter 4 we derive kinetic equations and study the nucleation and growth of micelles in systems out of equilibrium. In Chapter 5 we summarize the main results of this work and put emphasis on their possible experimental implications.

Chapter 2

Free Energy of a Solution of Amphiphilic Molecules

This chapter presents a new simple thermodynamic model of micellar aggregation. Its main advantage over the previous approaches presented in Sec. 1.3.2 is that it can be easily extended to treat more complicated issues, such as metastable states and various kinetic pathways. Indeed, the free energy function derived in this chapter serves as the starting point for the investigations presented in the following chapters. The model is based on the framework of first-order phase transitions, where the solution can be in one of two states — a monomeric state or an aggregated state, which contains both monomers and aggregates. The micelles themselves are treated as "droplets" (see Sec. 1.6.1), yet, due to the structure of the amphiphiles (Sec. 1.2), they cannot grow to infinite size, unlike nuclei of a macroscopic phase.

In Sec. 2.1 we derive an expression for the free energy of an amphiphilic solution. In Sec. 2.2 we obtain equations for the stationary points of the free energy and examine the free energy landscape and its consequences. In Sec. 2.3 we show how the free energy can be used to address properties of a single aggregate. [1]

[1] The material presented in this chapter was published in Ref. [56].

2.1 Derivation of the free energy

We use a two-state model, *i.e.*, assume that the solution can contain only two species — free monomers and micelles of $m > 1$ monomers. We thus neglect effects of polydispersity. (This crude approximation is justified, at least qualitatively, in the case of aggregation into sufficiently large ($m > 20$, say) globular micelles, where polydispersity is small [2].) We shall return to the issue of polydispersity in Sec. 3.4. Nonetheless, unlike earlier mass-action approaches [2, 9], we do not predefine an aggregated state of fixed size but rather treat m as a degree of freedom.

We define the model within the canonical ensemble, *i.e.*, fixing the temperature T, volume V, and total number of amphiphiles N. The number of free monomers is denoted by N_1, and the number of micelles by N_m, such that $N_1 + mN_m = N$. We use a Flory-Huggins lattice scheme [49] (see Sec. 1.5) with a lattice constant a, where each monomer occupies n lattice cells, i.e., a volume $v_1 = na^3$. Micelle formation is assumed to conserve the amphiphile volume, i.e., the volume of a micelle is $v_m = mv_1$. Hence, the volume fraction of free amphiphiles and those participating in micelles are, respectively, $\phi_1 = N_1 v_1/V$ and $\phi_m = N_m v_m/V$, such that the total volume fraction of amphiphiles, $\phi = \phi_1 + \phi_m = Nv_1/V$ is fixed.

Using these definitions, we write the free energy in units of the thermal energy $k_\mathrm{B}T$ as

$$\begin{aligned} F_\mathrm{tot} &= N_1 F_1 + N_m F_m + F_\mathrm{w}, \\ F_1 &= \ln \phi_1, \\ F_m &= \ln \phi_m - mu(m), \\ F_\mathrm{w} &= \frac{V}{a^3}(1-\phi)\ln(1-\phi). \end{aligned} \tag{2.1}$$

In Eq. 2.1 F_1 is the free energy of a monomer, assuming ideal entropy of mixing. The free energy of a micelle of size m, F_m, contains a similar contribution from translational entropy, while all other contributions to the free energy of transfer of a monomer from solution to an aggregate of size m are lumped into a single phenomenological function, $u(m)$. (A positive $u(m)$ corresponds to favorable aggregation.) The last term in Eq. 2.1, F_w, describes the entropy of mixing of the water molecules, whose volume fraction

is $(1-\phi)$. Expressing all of the variables in $F_{\rm tot}$ in terms of ϕ and ϕ_1, and dividing by V/a^3, we get the free energy density (per lattice site),

$$F(\phi_1,m,\phi)=\frac{a^3}{V}F_{\rm tot}=\frac{1}{n}\left(\phi_1\ln\phi_1+\frac{\phi-\phi_1}{m}\left[\ln(\phi-\phi_1)-mu(m)\right]\right)+(1-\phi)\ln(1-\phi). \tag{2.2}$$

Equation 2.2 serves as our main tool throughout this work. The partition of amphiphiles between monomers and aggregates (i.e., ϕ_1 and $\phi_m=\phi-\phi_1$), as well as the aggregation number m, are treated as degrees of freedom to be determined at equilibrium by minimization of F. The resulting equations are similar (yet not identical) to those obtained in Ref. [57].

This model has a single input in the form of the free energy of transfer, $u(m)$. Previous micellization theories derived the free energy of transfer based on detailed molecular arguments (e.g., Refs. [13]–[16],[19]). In the current work we prefer to remain on a more general level. The specific choice of $u(m)$ is not crucial for our qualitative results, as long as this function has a single maximum at a certain aggregation number. However, for the sake of concrete numerical examples, to be given later on, we shall use the following expression (already proposed in Ref. [57]):

$$u(m)=u_0-\sigma m^{-1/3}-\kappa m^{2/3}. \tag{2.3}$$

The first term in Eq. 2.3 represents a size-independent attraction among amphiphiles, where $u_0>0$ is the energy of this attraction in units of $k_{\rm B}T$. Since the attraction arises from the hydrophobic effect, u_0 is roughly proportional to the number of hydrocarbon groups in the amphiphile, $u_0\sim n$ [1]. The second term accounts for the surface energy of the aggregate, where $\sigma\sim n^{2/3}a^2\gamma/k_{\rm B}T$, γ being the surface tension between water and the micellar hydrophobic core. (Typically $a^2\gamma/k_{\rm B}T$ is of order unity.) Since the aggregate area scales as $m^{2/3}$, this contribution (per molecule) is proportional to $m^{-1/3}$. With the first two terms only, $u(m)$ is an increasing function of m, and the model yields a macroscopic condensation.[2] The third term in Eq. 2.3 is therefore introduced to produce finite aggregation numbers. This stabilizing term is assumed quadratic in the strained length of the amphiphile in the aggregate, i.e., it is quadratic

[2]Note the analogy to Eq. 1.12 in Sec. 1.6.1

in the aggregate radius, which scales as $m^{1/3}$. For example, if the hydrocarbon tail of the amphiphile is taken as a Gaussian chain, one expects $\kappa \sim n^{-1}$. Thus, there is actually little freedom in choosing values for the three parameters of $u(m)$ apart from changing n. Requiring the cmc and aggregation number to be of the right orders of magnitude further constrains these parameters.

2.2 Free energy landscape

Setting to zero the derivative of F in Eq. 2.2 with respect to ϕ_1 at fixed m leads to the following equation:[3]

$$\phi_1^m e^{mu(m)+m-1} = \phi - \phi_1, \tag{2.4}$$

whose solution is denoted $\phi_1^{\min}(m, \phi)$. Equation 2.4 has a unique solution which, for any m and ϕ, is a minimum of F along the ϕ_1 axis and is never larger than the total volume fraction ϕ, as required.[4] Setting to zero the derivative of F in Eq. 2.2 with respect to m at fixed ϕ_1 results in

$$m^2 = -\ln(\phi - \phi_1)/u'(m), \tag{2.5}$$

where a prime denotes a derivative with respect to m. Combining Eqs. 2.4 and 2.5 yields the following equations for the stationary (minimum or saddle) points of the free energy:

$$m^2 = -\ln[\phi - e^{-u(m)-mu'(m)-1+1/m}]/u'(m), \tag{2.6}$$

$$\phi_1 = e^{-u(m)-mu'(m)-1+1/m}. \tag{2.7}$$

Given a certain function $u(m)$ for the free energy of transfer (e.g., Eq. 2.3), we find the stationary points by first solving Eq. 2.6 for $m(\phi)$ and then substituting the solution in Eq. 2.7 to obtain $\phi_1(\phi)$. As the total amphiphile volume fraction ϕ is increased, the

[3] A similar equation is obtained from mass-action considerations [2, 57]. An extra factor of $m^{-1}e^{m-1}$ appears in Eq. 2.4, however, which originates from a more careful treatment of the mixing entropy in the Flory-Huggins analysis. Nonetheless, the dominant (exponential) part of this factor can be absorbed into u_0, and, therefore, the difference between the two approaches is minor.

[4] Note that for $m = 1$ one gets from Eq. 2.4 $\phi_1^{\min}$ smaller rather than equal to ϕ; this is an artifact of our two-state model, which distinguishes between monomers and "monomeric micelles" of $m = 1$.

free-energy landscape $F(\phi_1, m)$ qualitatively changes. Five distinct regimes are found, as described below. (See also Fig. 2.1.)

For sufficiently low volume fraction, $\phi < \varphi_1$, F has no stationary point, and its global minimum is given by the monomeric state, $m = 1$ (Fig. 2.1A). For $\phi > \varphi_1$ two stationary points appear (Fig. 2.1B) — a saddle point at $(\phi_1^{\min}(m^{\max}, \phi), m^{\max})$ and a local minimum at $(\phi_1^{\min}(m^{\min}, \phi), m^{\min})$. Thus, φ_1 is a spinodal-like concentration, at which a metastable aggregated state first appears.[5] The equation for φ_1 is

$$\varphi_1 = e^{-m^2 u'(m)} + e^{-u(m) - m u'(m) - 1 + 1/m}, \tag{2.8}$$

where m is the solution of the equation

$$m^3 u''(m) + 2m^2 u'(m) + 1 = 0. \tag{2.9}$$

(In deriving Eq. 2.9 we have assumed that at φ_1 the volume fraction of amphiphiles in micelles is much lower than that of the monomers, $\varphi_1 - \phi_1 \ll \phi_1$.) For the specific choice of $u(m)$ as given by Eq. 2.3, Eq. 2.9 becomes

$$10\kappa m^{5/3} - 2\sigma m^{2/3} - 9 = 0. \tag{2.10}$$

The appearance of the second free-energy minimum for $\phi > \varphi_1$ may cause parts of the solution to be trapped for some time in this metastable state. This possibility and its consequences will be studied in detail in Chapter 3. Here we will only point out that the occupancy of the metastable state close to φ_1 is very small and becomes appreciable only above a higher concentration $\varphi_2 > \varphi_1$ (Fig. 2.1C).

Above another, higher, value of the volume fraction, $\varphi_3 > \varphi_2$, the free energy difference between the two states reverses sign, and the aggregated state (containing both monomers and aggregates) becomes the global minimum (Fig. 2.1D). Thus, φ_3 is a binodal-like point, above which the state with aggregates is favorable whereas the pure monomeric state becomes metastable.

[5] Note that, since ϕ_1 and m are free thermodynamic variables, the appearance of a second free-energy minimum does not correspond to equilibrium coexistence between the two states. The pure monomeric state, which is the global minimum of F, remains the stable one. The aggregated state, which in itself consists of coexisting monomers and aggregates, is metastable.

The two stable/metastable states are separated by a saddle point of F at $[\phi_1^{\min}(m^{\max}), m^{\max}]$. For any reasonable form of $u(m)$, the aggregate size at the saddle point, $m^{\max}$, (i.e., the critical nucleus) decreases with ϕ and at a certain amphiphile volume fraction, $\varphi_4 > \varphi_3$, it becomes equal to 1. Thus, φ_4 represents a second spinodal-like point, above which the metastable monomeric state becomes unstable and the aggregated state remains the sole free-energy minimum (Fig. 2.1E).

Figure 2.1 shows cuts of the free-energy landscape along the $\phi_1^{\min}(m)$ line as a function of aggregation number m in the five regimes. The values of parameters used in the figure characterize a representative surfactant, which will serve as a consistent example throughout the various parts of the thesis. (See Tables 3.1 and 4.1 later on.)

To summarize, the free energy derived in Sec. 2.1 yields a sequence of four well separated values of volume fraction, $\varphi_1 < \varphi_2 < \varphi_3 < \varphi_4$, corresponding to points of qualitative changes in the thermodynamic behavior of the surfactant solution. Of these four values, as we shall see in the next chapter, φ_3 is the one corresponding to the commonly defined cmc.

2.3 Treating single-aggregate properties

Since our model does not explicitly consider single micelles but macrostates containing both micelles and monomers, a certain volume of solution needs to be specified to allow the calculation of various properties of a single aggregate. The relevant sub-volume, V_s, is the one that contains (on average) one aggregate of size m. The volume of the aggregate itself is na^3m, and the volume fraction of aggregates is $\phi - \phi_1$. Hence, the relevant subsystem volume is

$$V_s(m, \phi) = \frac{na^3 m}{\phi - \phi_1^{\min}(m)}. \tag{2.11}$$

Since $\phi - \phi_1$ in a micellar solution is typically very small, V_s is far from being microscopic, and we may apply our coarse-grained description to the subsystem. In other words, instead of treating a single aggregate, we treat a subsystem of volume V_s, which

is in the aggregated state. The free energy to be treated is, therefore,

$$F_s(\phi_1, m, \phi) = \frac{V_s}{a^3} F. \tag{2.12}$$

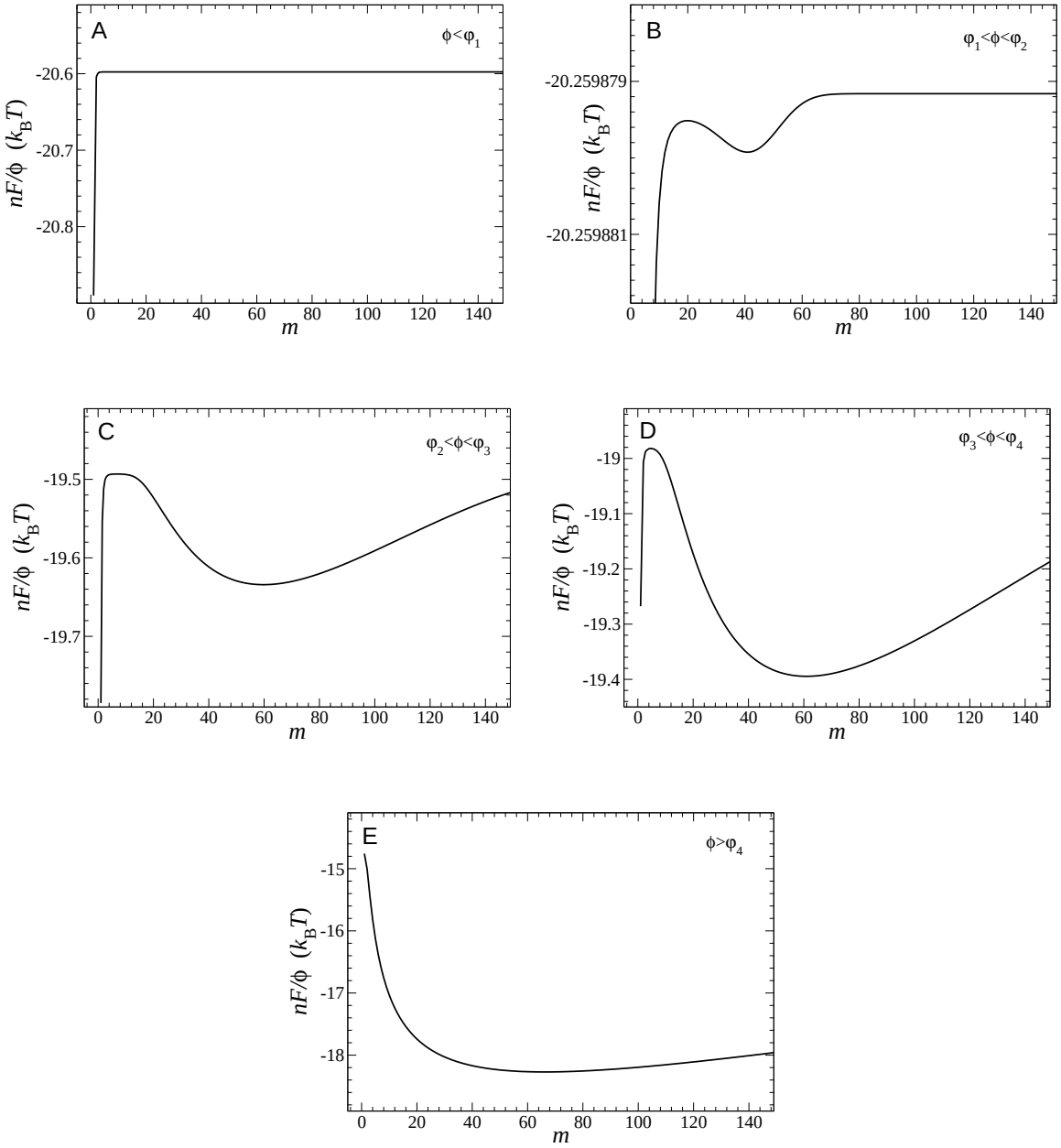

Figure 2.1: Free energy per amphiphile along the $\phi_1^{\min}(m)$ line as a function of aggregation number for $\phi = 0.0005 < \varphi_1$ (panel A), $\varphi_1 < \phi = 0.0007 < \varphi_2$ (panel B), $\varphi_2 < \phi = 0.0015 < \varphi_3$ (panel C), $\varphi_3 < \phi = 0.0025 < \varphi_4$ (panel D), and $\phi = 0.11 > \varphi_4$ (panel E). The parameters of F are shown in Table 3.1 (Amphiphile A).

Chapter 3

Premicellar Aggregation of Amphiphilic Molecules

In this chapter we apply the free energy formalism derived in Chapter 2 to the study of premicellar (metastable) aggregation in amphiphilic solutions. [1].

3.1 Introduction

The question of how critical the cmc is has been a long-standing controversy in the field. During the years there were several experimental indications (e.g., [59, 60]), as well as theoretical ones (e.g., [61]), for the appearance of aggregates at concentrations well below the cmc — a phenomenon referred to as *premicellar aggregation* — yet the overall results remained inconclusive. In a recent experiment Zettl et al. applied fluorescence correlation spectroscopy (FCS) for the first time to study self-assembly in surfactant solutions [62]. Their measurements indicated the existence of micelles at surfactant concentrations down to four times lower than the macroscopically determined cmc. They also inferred that the aggregates had roughly the same size below and above the cmc. Recent NMR experiments on surfactant solutions (Refs. [63] and [64]) observed premicellar aggregation as well.

The model presented in Chapter 2, despite its apparent simplicity, allows us for the first time to address metastable aggregates in detail and thus examine the extent of

[1] The material presented in this chapter was published in Refs. [56] and [58]

premicellar aggregation. In the following sections of this chapter we will give a definition of the cmc similar to the experimental one and examine the extent of premicellar aggregation using numerical examples.

3.2 Thermodynamics of premicellar aggregation

The equilibrium properties of a solution of amphiphilic molecules are determined by minimization of the free energy, Eq. 2.2.

3.2.1 Fixed aggregation number

Before proceeding to the full examination of the free energy landscape presented in Chapter 2, it is instructive to examine the behavior in the case of aggregates of fixed size. This simpler situation is equivalent to the one described by a two-state mass-action model [9]; [2] the only freedom left is the partition of the amphiphiles between two fixed states.

If m is taken as a fixed parameter, F is a function of ϕ_1 alone, and the free energy of transfer is a constant, $u(m) = u$. The global minimum of F is then at $\phi_1^{\min} < \phi$, as given by Eq. 2.4. Thus, in this case aggregates exist at any amphiphile concentration. We characterize the extent of aggregation by the fraction of molecules participating in micelles, $x \equiv (\phi - \phi_1)/\phi$, which can be found as a function of ϕ by substituting the solution for $\phi_1^{\min}$. An example is given in Fig. 3.1, where $x(\phi)$ as well as the monomer volume fraction, $\phi_1 = (1-x)\phi$, are presented. Although in this case $x > 0$ for any ϕ, there is a well defined value of $\phi = \phi^{\mathrm{cmc}}$ above which aggregation becomes appreciable. In accord with the experimental determination of the cmc described in Sec. 1.3.1, we define this cmc as the point of maximum curvature ("knee") of $(1-x)\phi$ as a function of ϕ, i.e., as the solution of the equation $\partial^3\phi_1^{\min}/\partial\phi^3 = 0$ (dotted line in Fig. 3.1). The fraction of amphiphiles participating in micelles just below the cmc, $x^{\mathrm{cmc}}(m) = x(\phi^{\mathrm{cmc}}(m))$, can be used to characterize the extent of premicellar

[2] See, for example, the treatment of Ref. [6] for the case of the reaction $mA_1 \underset{k^-}{\overset{k^+}{\rightleftharpoons}} A_m$.

aggregation. Using Eq. 2.4 and the above definition of the cmc, we find

$$\text{fixed } m: \qquad x^{\mathrm{cmc}}(m) = \frac{m-2}{2(m^2-1)}, \tag{3.1}$$

i.e., $x^{\mathrm{cmc}} \sim 1/m$ for realistic aggregation numbers, $m \gg 1$.

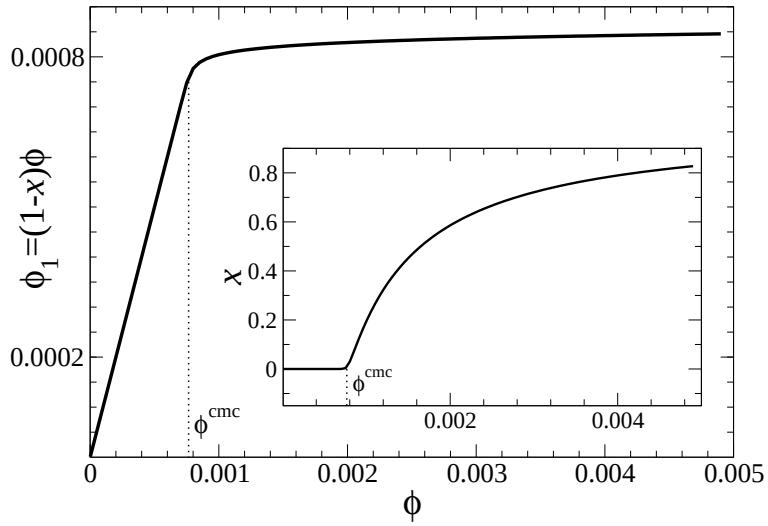

Figure 3.1: Monomer volume fraction as a function of total volume fraction for fixed $m = 60$ and $u_0 = 10$, $\kappa = 0.08$, $\sigma = 11$. The inset shows the fraction of amphiphiles participating in micelles.

In the special asymptotic case of $m \to \infty$ (while requiring that $u(m)$ remain finite), the results above reduce, as expected, to a discontinuous, macroscopic phase transition: for $\phi < \phi_c = e^{-u-1}$ the global minimum of F is at $\phi_1 = \phi$, i.e., the system is in a pure monomeric state, whereas for $\phi > \phi_c$ the monomer volume fraction remains fixed at ϕ_c, and any additional amphiphiles go into the macroscopic aggregate. The "knee" defining the cmc in Fig. 3.1 turns into a singular "corner", and x^{cmc} vanishes. From this perspective the picture obtained above for a finite, fixed aggregation number (the existence of aggregates at any ϕ, the non-zero premicellar aggregation $x \sim 1/m$) is merely a manifestation of a phase transition smoothed by finite-size effects (finite m) [65]. As will be shown in the next section, this picture significantly changes when the aggregation number is free to vary with amphiphile concentration.

3.2.2 Variable aggregation number

We now proceed to the more realistic scenario where the aggregation number is a degree of freedom. Throughout this section we shall demonstrate the resulting aggregation behavior using two numerical examples, corresponding to two choices of parameters for $u(m)$ of Eq. 2.3 (see Table 3.1). (The parameter values have been chosen to mimic two amphiphiles differing in their hydrocarbon tail length n by a factor of about 3/2, using the qualitative dependencies on n discussed in Sec. 2.1.)

Table 3.1: Parameters and equilibrium properties of exemplary amphiphiles. n — number of groups in hydrocarbon tail; u_0, σ, κ — parameters of $u(m)$; φ_1 — first spinodal-like point; φ_2, φ_3 — volume-fraction bounds of the premicellar regime; $\omega(\varphi_2)$, $\omega(\varphi_3)$ — relative width of micelle size distribution at these boundaries.

Amphiphile	n	u_0	σ	κ	φ_1	φ_2	φ_3	$\omega(\varphi_2)$	$\omega(\varphi_3)$
A	13	10	11	0.08	6.6×10^{-4}	8.0×10^{-4}	2.0×10^{-3}	0.18	0.15
B	20	14	14	0.05	1.2×10^{-5}	1.6×10^{-5}	6.7×10^{-5}	0.11	0.10

As noted in Chapter 2 the appearance of the second free-energy minimum for $\phi > \varphi_1$ may cause parts of the solution to be trapped for some time in the metastable aggregated state. At equilibrium the number of metastable aggregates will depend on the free energy difference between the two minima at $m = m^{\min}$ and at $m = 1$, [3]

$$\Delta F(\phi) = F[\phi_1^{\min}(m^{\min}), m^{\min}, \phi] - F[\phi_1^{\min}(m = 1), m = 1, \phi]. \tag{3.2}$$

The free energy difference per amphiphile is $n\Delta F/\phi$. As seen in Fig. 3.2 for our two characteristic examples, it is comparable to or smaller than $k_{\mathrm{B}}T$. For other choices of parameters it may reach larger values, yet not exceeding a few $k_{\mathrm{B}}T$. (Examination of the equations reveals that this energy scale relates to the value of $u(m)$ at small aggregation number.) These low values of $n\Delta F/\phi$ imply that significant occupancy of the metastable state (i.e., premicellar aggregation) may be obtained at full equilibrium.

To check the extent of this effect, we calculate the fraction x of amphiphiles participating in metastable micelles. The occupancy probability of the "excited" state is

[3] The second term in Eq. 3.2 is not strictly equal to the free energy of the monomeric state, $F(\phi_1 = \phi)$, due to the artifact mentioned in Sec. 2.2 (footnote 4). This slight difference, however, does not affect the results.

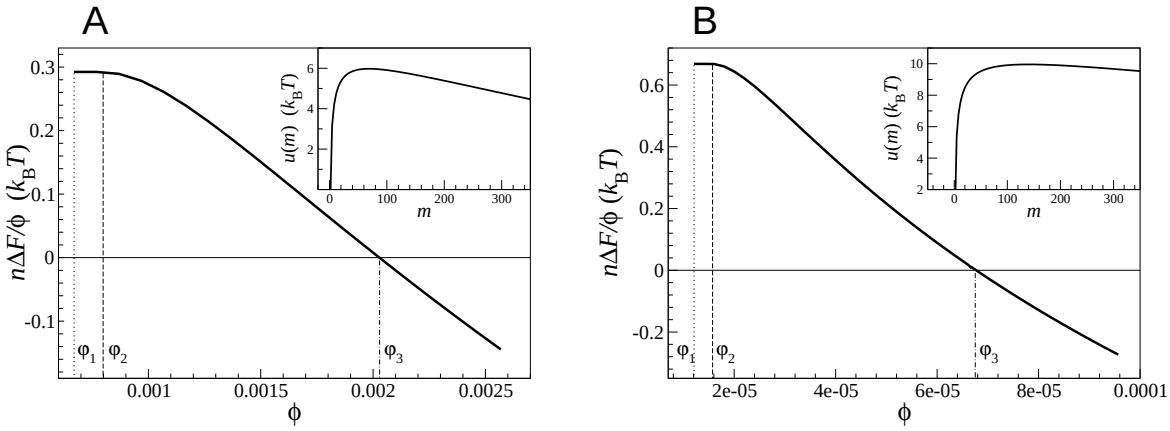

Figure 3.2: Free energy difference per amphiphile (in k_BT units) between the monomeric and aggregated states as a function of total amphiphile volume fraction for the numerical examples of Table 3.1. These two examples mimic two amphiphiles differing in their tail length, n, by a factor of 3/2, (B) being the more hydrophobic one. (See text in Sec. 2.1).

$\exp(-n\Delta F/\phi)/[1+\exp(-n\Delta F/\phi)]$, leading to

$$x(\phi) = \begin{cases} 0, & \phi < \varphi_1 \\ \frac{\phi - \phi_1^{\min}(m^{\min})}{\phi} \frac{\exp(-n\Delta F/\phi)}{1+\exp(-n\Delta F/\phi)}, & \phi > \varphi_1. \end{cases} \tag{3.3}$$

The results for $x(\phi)$ are shown in Fig. 3.3. Over a concentration range above φ_1 x remains negligible (insets of Fig. 3.3). Comparing with Fig. 3.2, we see that in this range the free energy difference between the states hardly changes. Figure 3.4 presents the change in the favorable aggregation number as a function of ϕ, demonstrating that this region of negligible aggregation is characterized by a rapid increase in $m^{\min}$.

At a well defined volume fraction, $\phi = \varphi_2$, x starts to increase significantly, i.e., an appreciable amount of metastable, premicellar aggregates forms (Fig. 3.3). Thus, φ_2 marks the onset of premicellar aggregation. In Fig. 3.4 we see that in this region the aggregation number crosses over to a much weaker dependence on ϕ. Premicellar aggregation occurs, therefore, when the favorable aggregation number stops increasing significantly. We define φ_2 accordingly as the volume fraction at which $d^3m^{\min}/d\phi^3 = 0$ (dashed vertical lines in the figures).

Equation 3.3 for x remains correct in the region above φ_3 (the binodal-like point)

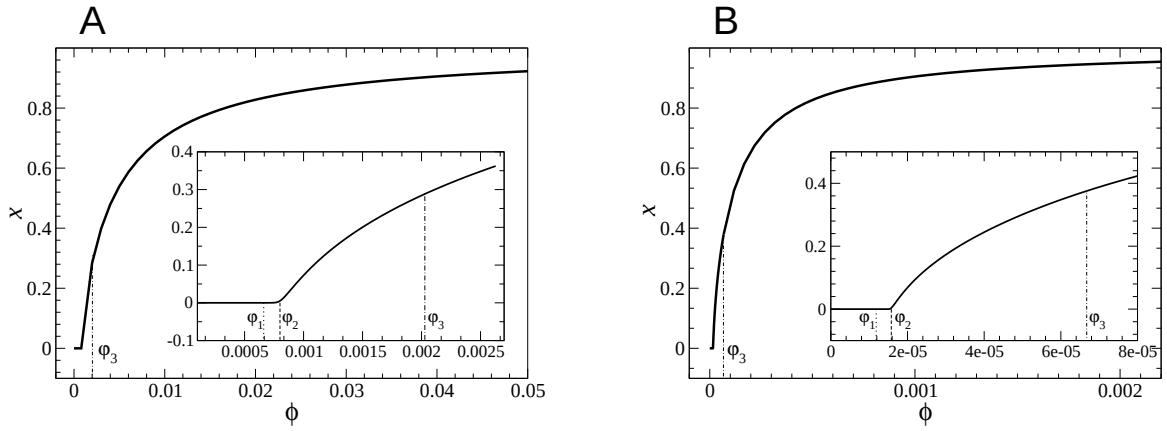

Figure 3.3: Fraction of amphiphiles in micelles as a function of total volume fraction for the examples of Table 3.1.

as well (Sec. 2.2). Combining Eqs. 2.4, 2.6, 2.7, and 3.2, we calculate φ_3 by setting $\Delta F(\varphi_3) = 0$ (dash-dotted vertical lines in the figures). In our examples the concentration at which metastable aggregates begin to form (φ_2) is about 2–4 times lower than the one at which they become favorable (φ_3).

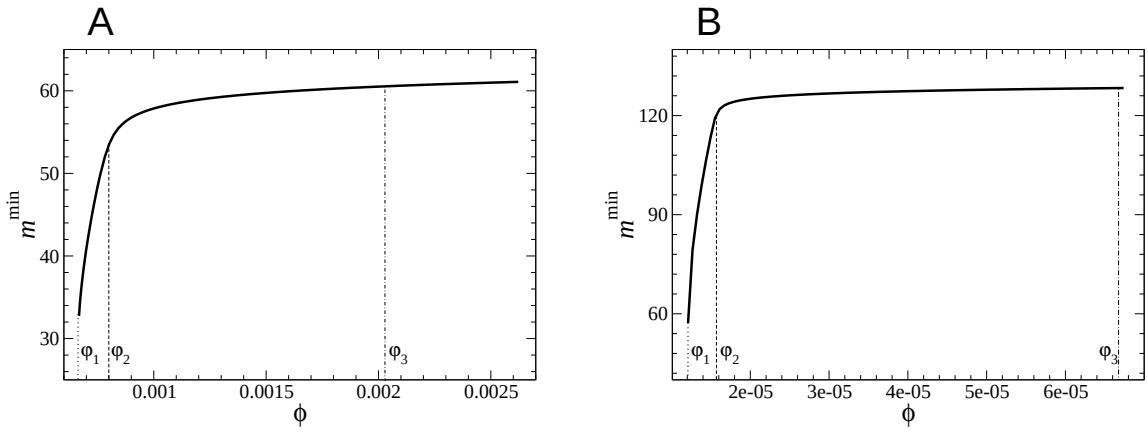

Figure 3.4: Aggregation number as a function of total volume fraction for the examples of Table 3.1.

The volume fraction of monomers in the solution, $\phi_1 = (1 - x)\phi$, obtained using Eq. 3.3, is of experimental interest since, e.g., it is directly related to the commonly measured conductivity in ionic surfactant solutions. Figure 3.5 shows the plots of ϕ_1 as a function of ϕ. For $\phi < \varphi_2$ there are essentially no aggregates, and the volume fraction of monomers is equal to the total one (insets). The slight change in curvature

at $\phi = \varphi_2$ indicates the beginning of premicellar aggregation. Experimentally the cmc is usually extracted from such curves by interpolating the behaviors at low and high concentrations (Sec. 1.3.1), i.e., it corresponds to the "knee" in the curves of Fig. 3.5. As can be seen in the figure, when a sufficiently wide range of ϕ is examined, the cmc so determined is close to φ_3, our binodal-like point. Note that just below the cmc the fraction of amphiphiles participating in (metastable) micelles (Fig. 3.3) has already reached tens percent. This extent of premicellar aggregation (Fig. 3.3A) is 1–2 orders of magnitude larger than the one obtained in Sec. 3.2.1 for the same m and $u(m)$ while assuming a fixed aggregation number (Eq. 3.1 and Fig. 3.1).

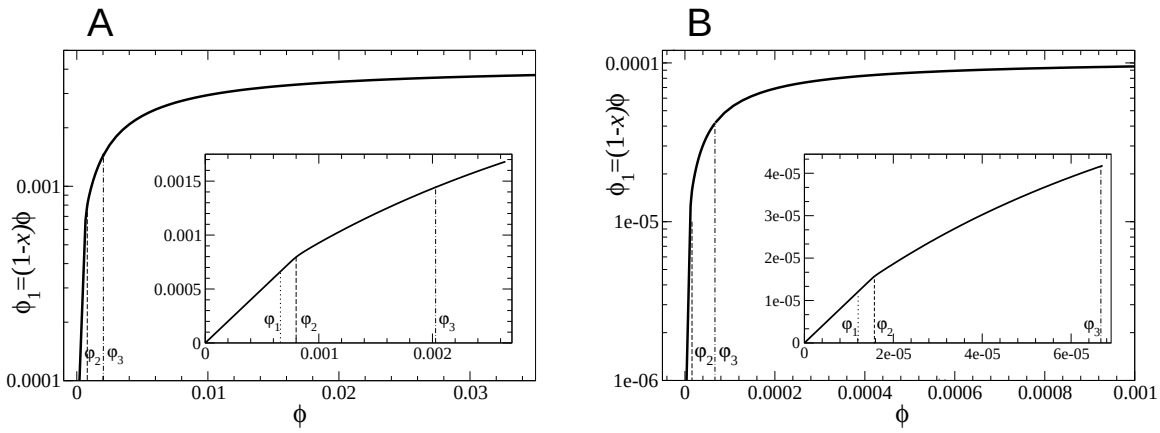

Figure 3.5: Monomer volume fraction as a function of total volume fraction for the examples of Table 3.1.

Thus, provided that the solution reaches full equilibrium, we find that in the range $\varphi_2 < \phi < \varphi_3$ it should contain an appreciable amount of premicelles. However, there are three issues that might affect the experimental relevance of premicellar aggregates: (a) the aggregation may be kinetically hindered by high nucleation barriers; (b) the distribution of premicellar sizes may be much broader than that of regular micelles; (c) the lifetime of premicelles may be too short. These issues are addressed in the following three sections.

3.3 Kinetic barriers to premicellar aggregation

Our treatment of the metastable aggregates so far has been an equilibrium one, involving the free energy difference between the stable and metastable states. In reality the extent of such premicellar aggregation may be affected by kinetic limitations arising from the free energy (nucleation) barrier between the two states. As described earlier, the nucleation barrier can be obtained from the current model as well; it is given by the other stationary (saddle) point of F, as found from Eqs. 2.6 and 2.7 for $\phi > \varphi_1$. (See Fig. 2.1C.)

To calculate the nucleation barrier *per aggregate*, *i.e.*, the free energy (in units of $k_{\mathrm{B}}T$) required to form a nucleus of size $m^{\max}$, we employ the approach presented in Sec. 2.3, resulting in Eq. 2.11. for the volume per aggregate, V_s. The nucleation barrier is given then by

$$\Delta F^{\mathrm{nuc}}(\phi) = \frac{V_s(m^{\max},\phi)}{a^3}[F(\phi_1^{\min}(m^{\max}), m^{\max}, \phi) - F(\phi_1^{\min}(m=1), m=1, \phi)], \quad (3.4)$$

with the saddle point $(\phi_1^{\min}, m^{\max})$ found from Eqs. 2.6 and 2.7. The results for our two examples are shown in Figs. 3.6 and 3.7. As can be seen in Fig. 3.7 the nucleation barriers in both examples are very high, implying that homogeneous nucleation of premicellar aggregates is kinetically hindered. The consequences of this for premicellar aggregation, as well as for regular micellization, will be further discussed in Sec. 3.6. The large nucleation barriers for both examples stem from the low concentration of critical nuclei, $V_s(m^{\max},\phi)^{-1}$ (Eqs. 2.11 and 3.4). ΔF^{nuc} decreases rapidly with ϕ due to the increase of critical nuclei concentration, and also because of the decrease in the critical-nucleus size, $m^{\max}$ (Fig. 3.6). The example in Fig. 3.7B, for which the aggregation numbers are roughly double, exhibits a much higher (physically insurmountable) barrier than the one of Fig. 3.7A. As the amphiphile volume fraction is increased, both $m^{\max}$ and ΔF^{nuc} decrease monotonously. Hence, at a sufficiently large $\phi > \varphi_4$ (not shown in the graphs), the energy barrier disappears, indicating a second spinodal-like point, where the aggregated state is the only stable one.

Comparison between our two selected examples (panels A and B in Figs. 3.2–3.7) reveals that the more hydrophobic amphiphile (larger n, panels B) exhibits the follow-

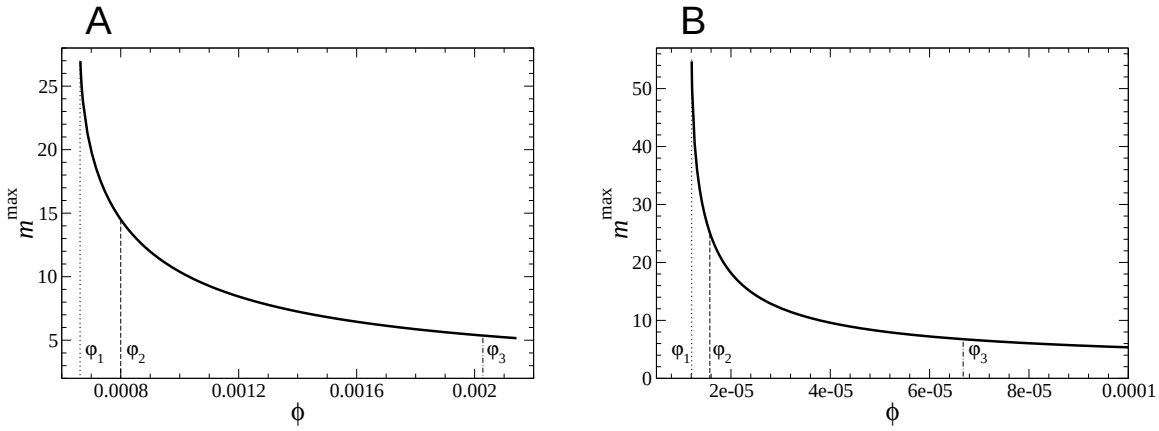

Figure 3.6: Critical nucleus size as a function of total volume fraction for the examples of Table 3.1.

ing: (i) larger aggregation number; (ii) lower cmc, φ_3; and (iii) larger critical nucleus, $m^{\max}$, and nucleation barrier, ΔF^{nuc}. These are the expected trends for amphiphilic self-assembly. In addition, we note that the relative width of the premicellar region, $(\varphi_3 - \varphi_2)/\varphi_3$, is comparable for the two examples.

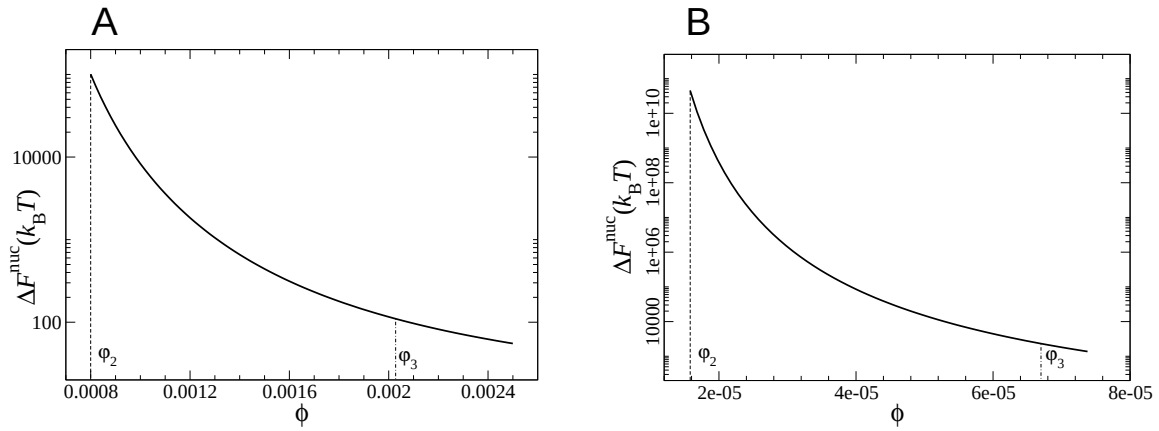

Figure 3.7: Nucleation barrier (in $k_{\mathrm{B}}T$ units) as a function of total volume fraction for the examples of Table 3.1.

3.4 Polydispersity of premicellar aggregates

Although the mean size of premicellar aggregates (once they somehow manage to form, e.g., via heterogeneous nucleation) has been found to be similar to that of the

micelles above the cmc, the size distribution in the former case might be broader. Evidently, this could jeopardize the experimental and technological relevance of premicellar aggregation. We should therefore examine the aggregate size fluctuations in the premicellar regime.

For a given amphiphile volume fraction in the premicellar regime, $\varphi_2 < \phi < \varphi_3$, the aggregation number of the metastable aggregates, $m^{\min}(\phi)$, is given by the local minimum of the free energy F. To examine the polydispersity of the aggregates we calculate the fluctuations of m around $m^{\min}$ for a single aggregate. We calculate the free energy of the aggregate using Eqs. 2.11 and 2.12 while neglecting changes in the volume per aggregate, $V_s(m,\phi) \simeq V_s(m^{\min},\phi)$. The free energy of the subsystem is, therefore,

$$F_s(\phi,m) = \frac{V_s(m^{\min},\phi)}{a^3} F(\phi_1^{\min}(m),m,\phi). \tag{3.5}$$

The equilibrium distribution of m in that subsystem can be assumed proportional to the Boltzmann factor, $e^{-F_s(m)}$. Since the biggest contributions to the micelle size distribution come from values close to $m^{\min}$, we can expand $F_s(m)$ around $m^{\min}$. The resulting normalized equilibrium distribution of m around $m^{\min}$ is given by

$$f(m) \simeq \left[F_s''(m^{\min})/(2\pi)\right]^{1/2} e^{-\frac{1}{2}F_s''(m^{\min})(m-m^{\min})^2}, \tag{3.6}$$

where a prime denotes a derivative with respect to m. Thus, we readily get for the mean-square size fluctuation,

$$\langle \delta m^2 \rangle = 1/F_s''(m^{\min}). \tag{3.7}$$

The relative width of the size distribution,

$$w = \frac{\langle \delta m^2 \rangle^{1/2}}{\langle m \rangle} = \frac{1}{m^{\min}[F_s''(m^{\min})]^{1/2}}, \tag{3.8}$$

provides a convenient measure of the polydispersity.

Figure 3.8 shows the mean-square fluctuation of the aggregation number for amphiphile A (Table 3.1) as a function of volume fraction. The corresponding relative width of the aggregate size distribution is presented in the inset. The polydisper-

sity weakly decreases with concentration, *i.e.*, the premicellar aggregates are nearly as monodisperse as the micelles above the cmc. In Table 3.1 we see that the same conclusions hold for amphiphile B. The small polydispersity (around 10%), as well as the slightly increased value for the less hydrophobic amphiphile (A), are in agreement with the well known trends for spherical micelles above the cmc, as established experimentally [11] and theoretically [2].

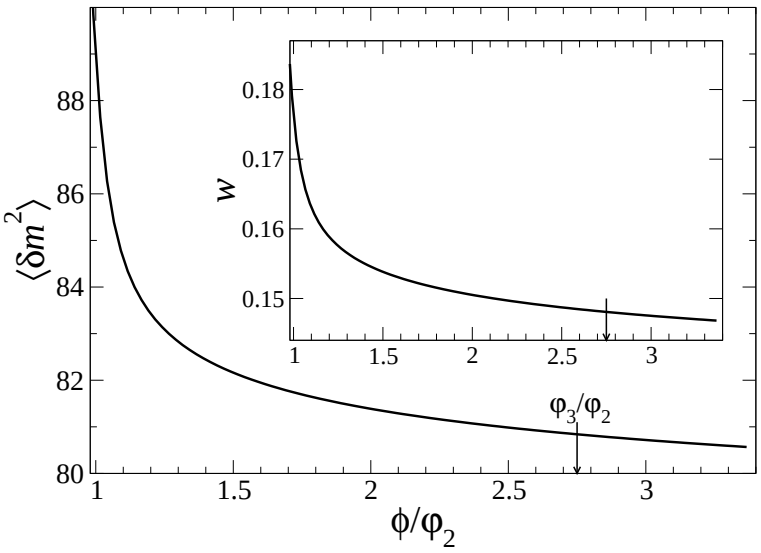

Figure 3.8: Mean-square fluctuation of aggregation number for amphiphile A as a function of amphiphile volume fraction. The volume fraction is scaled by φ_2, the onset of premicellar aggregation. The cmc (φ_3) is indicated by an arrow. The inset shows the relative width of the aggregate size distribution, $w = \langle \delta m^2 \rangle^{1/2} / \langle m \rangle$. Parameters of amphiphile A are given in Table 3.1.

3.5 Lifetime of the premicellar aggregates

The third issue, pertaining to the experimental relevance of premicelles, concerns their lifetime, assuming that the solution has fully equilibrated and premicellar aggregates have formed. While the metastable premicellar state may be appreciably occupied at equilibrium (Sec. 3.2), the aggregates might be short-lived.

As mentioned in Sec. 1.4, two disparate time scales are involved in the dynamics of micelles, corresponding to the exchange of individual monomers between the micelle and the solution and the much slower process of micelle formation and breakup. Being

interested in aggregate stability, we focus here on the latter. We use the free energy landscape, as obtained from the thermodynamic model (Chapter 2), within Kramers' rate theory [54, 55] (Sec. 1.6.2) to study the lifetime of premicellar aggregates.

The following analysis relies on two basic assumptions. First, we assume that overcoming the barrier at the saddle point $[\phi_1^{\min}(m^{\max}), m^{\max}]$ is the rate-limiting process in aggregate dissociation, whereas diffusion is much faster. Hence, the dynamics depend on m alone, advancing at all times t along the path $[\phi_1^{\min}(m(t)), m(t)]$. The second assumption arises from the necessity to relate our coarse-grained model with single-aggregate properties (see Sec. 2.3). We calculate the free energy of a premicellar aggregate using Eqs. 2.11 and 2.12, under the assumption that the volume per aggregate stays equal to $V_s(m^{\min}, \phi)$ throughout the process. The free energy of the subsystem becomes

$$F_s(\phi_1, m, \phi) = \frac{V_s(m^{\min}(\phi), \phi)}{a^3} F, \tag{3.9}$$

where F is given by Eq. 2.2. Thus, the dissociation of a single premicellar aggregate is treated as the transition of a mesoscopic subsystem from a metastable state, containing monomers and (on average) one aggregate, to the stable, purely monomeric state. For brevity the free energy of the subsystem along the dissociation path $[\phi_1^{\min}(m(t)), m(t)]$ is hereafter referred to simply as $F_s(m)$.

3.5.1 Model

We follow the lines of Kramers' theory [54, 55] (Sec. 1.6.2) while adapting it to the case of premicellar aggregates. The main assumptions of this approach are as follows. (i) The energy barrier between the two states is sufficiently high, leading to separation of time scales between the fast monomer exchange process and the much slower aggregate dissociation. (ii) The free energy of the final (monomeric) state is much lower than that of the initial (aggregated) one, ensuring a practically unidirectional probability current from the aggregated to the monomeric state. The first assumption breaks down when ϕ is too small, *i.e.*, as it gets too close to φ_1; in the examples of Sec. 3.5.2 it becomes invalid already for $\phi \simeq \varphi_2$. The second assumption fails when ϕ gets close to φ_3. Thus, the following calculation is strictly valid only for $\varphi_2 \ll \phi \ll \varphi_3$. (The behavior outside this domain of validity will be commented on separately in Sec.

3.6.) In addition, we assume that the aggregation number is large, $m \gg 1$, so that the discrete changes in m can be replaced to a good approximation by continuous, infinitesimal ones.

We begin with the master equation for the probability density function, $f(m,t)$, of finding the subsystem around the state $[\phi_1^{\min}(m), m]$ at time t,

$$\frac{\partial f(m,t)}{\partial t} = \int dk W(m-k,k) f(m-k,t) - \int dk W(m,k) f(m,t) dk, \tag{3.10}$$

where $W(m,k)$ is the transition probability per unit time for the aggregation number to change from m to $m+k$. Assuming that large jumps in aggregation number are improbable, we expand the first integral in Eq. 3.10 to second order in small k and get the Fokker-Planck equation,

$$\frac{\partial f}{\partial t} = -\frac{\partial j}{\partial m}, \quad j(m,t) = A(m) f(m,t) - \frac{\partial}{\partial m}[D(m) f(m,t)]. \tag{3.11}$$

The first term in the probability current density j describes a drift along the aggregation-number axis, with velocity $A(m) = \int dk k W(m,k)$. The second term represents diffusion along that axis, with a diffusion coefficient

$$D(m) = \frac{1}{2} \int dk k^2 W(m,k). \tag{3.12}$$

Demanding that f reduce at equilibrium (*i.e.*, when $j = 0$) to the Boltzmann distribution, $f_{\rm eq}(m) \sim e^{-F_s(m)}$, one gets from Eq. 3.11 a generalized Einstein relation between A and D,

$$A(m) = -D(m) F_s'(m) + D'(m), \tag{3.13}$$

where a prime denotes a derivative with respect to m. Substituting this relation back in Eq. 3.11, we rewrite the probability current density as

$$j = -D(m) e^{-F_s(m)} [f(m,t) e^{F_s(m)}]'. \tag{3.14}$$

Thanks to the assumed high free-energy barrier, and the resulting separation of time scales, steady state can be assumed practically throughout the entire dissociation

process. Thus, $\partial f/\partial t = \partial j/\partial m = 0$, *i.e.*, $j = j_{\rm ss}$ independent of m. Equation 3.14 can then be integrated over m,

$$j_{\rm ss}\int_1^{m^{\rm min}} dm\frac{e^{F_s}}{D} = -fe^{F_s}\Big|_1^{m^{\rm min}} . \tag{3.15}$$

The second assumption, of a large free-energy difference between the two states, implies that the right-hand side (rhs) of Eq. 3.15 is dominated by its value at $m^{\rm min}$. In addition, we assume that the subsystem is still mostly in the aggregated state near $m^{\rm min}$, at quasi-equilibrium, and, hence, $f(m,t) \sim e^{-F_s(m)}$. Expanding about $m^{\rm min}$ we obtain for the normalized probability density,

$$f(m) \simeq \left[F_s''(m^{\rm min})/(2\pi)\right]^{1/2} e^{-\frac{1}{2}F_s''(m^{\rm min})(m-m^{\rm min})^2}. \tag{3.16}$$

as already obtained in Sec. 3.4 (Eq. 3.6). The rhs of Eq. 3.15 is given, therefore, by $-[F_s''(m^{\rm min})/(2\pi)]^{1/2}e^{F_s(m^{\rm min})}$.

Treating the left-hand side (lhs) of Eq. 3.15 requires an estimate for the aggregation-number diffusion coefficient, $D(m)$. We use the definition of this coefficient, Eq. 3.12, together with Langer's formula for the transition probability [66],

$$W(m,k) \sim \tau_0^{-1}e^{-k^2/(2\Delta)}e^{-\frac{1}{2}[F_s(m+k)-F_s(m)]}, \tag{3.17}$$

where τ_0 is a molecular time scale, and Δ is used to suppress large jumps in the aggregation number. Assuming that jumps much larger than unity are improbable, we set $\Delta = 1$. We then expand $F_s(m+k) - F_s(m)$ in Eq. 3.17 to second order in k, normalize the transition probability, and substitute it in Eq. 3.12 to obtain

$$D(m) = \frac{1}{2\tau_0}\frac{4 + F_s'^2 + 2F_s''}{(2+F_s'')^2}. \tag{3.18}$$

Analysis of Eqs. 2.2, 2.3, 2.11, 3.9 and 3.18 shows that for realistic aggregation numbers, $m \gg 1$, one has $|F_s| \gg |\ln D|$. Hence, the integral on the lhs of Eq. 3.15 is dominated by a small region around the maximum of F_s. We expand $F_s(m)$ about $m^{\rm max}$, integrate, and get for the lhs of Eq. 3.15, $j_{\rm ss}[2\pi/|F_s''(m^{\rm max})|]^{1/2}e^{F_s(m^{\rm max})}/D(m^{\rm max})$.

Substituting all these results in Eq. 3.15, we finally obtain for the micelle lifetime [4],

$$\tau_{\rm m} = |j_{\rm ss}|^{-1} = \frac{4\pi\tau_0}{(1+F_s''(m^{\rm max})/2)\,|F_s''(m^{\rm min})F_s''(m^{\rm max})|^{1/2}} e^{F_{\rm b}}, \qquad (3.19)$$

where $F_{\rm b} = F_s(m^{\rm max}) - F_s(m^{\rm min})$ is the height of the free-energy barrier between the aggregated and monomeric states. Equation 3.19, combined with Eqs. 2.2, 2.3, 2.11 , yields the aggregate lifetime in the metastable, premicellar regime.

3.5.2 Results

We now demonstrate the results of the model for the numerical examples given in Table 3.1. It lists for these examples the volume-fraction bounds of the premicellar regime, φ_2 and φ_3. The aggregation numbers at these points, as obtained in Sec. 3.2, are given in Table 3.2.

In Table 3.2 we also give the values of the free-energy barrier for aggregate dissociation at the lower and upper bounds of the premicellar regime, as calculated from Eqs. 2.2, 2.3, 2.11 using the parameters of Table 3.1. At $\phi = \varphi_2$ the barrier is negligible, of order $k_{\rm B}T$, yet, as ϕ increases through the premicellar regime, it becomes much larger than $k_{\rm B}T$. The resulting lifetimes, as calculated from Eq. 3.19, are given in Table 3.2. As an estimate for the molecular time scale we have used for both amphiphiles $\tau_0 = 10$ ns. (This is the diffusion time of a molecule, having a diffusion coefficient of 10^{-6} cm^2/s, as it diffuses along a distance of 1 nm.) Corresponding to the increase in the free-energy barrier, the aggregate lifetime increases from milliseconds at the lower bound of the premicellar region to practically indefinite time. As already noted in Sec. 3.5.1, our lifetime analysis is strictly valid only for $\varphi_2 \ll \phi \ll \varphi_3$, and, hence, these values should be regarded merely as rough estimates.

The premicellar aggregate lifetime for amphiphile A, scaled by the molecular time τ_0, is depicted as a function of amphiphile volume fraction in Fig. 3.9. The roughly exponential increase of lifetime with concentration stems from the exponential de-

[4] For $F_s''(m^{\rm max}) \le -2$ this result evidently breaks down. In the representative examples of Sec. 3.5.2 we have $|F_s''(m^{\rm max})| < 0.1$. One can find examples where $|F_s''|$ approaches 2, yet this occurs only close to φ_3, the upper edge of the metastable region, where the Kramers-like approach becomes inappropriate. Technically, the divergence can anyway be avoided by reducing the value of the parameter Δ in Eq. 3.17.

Table 3.2: Properties of premicellar aggregates. $m^{\min}$—aggregation number; $F_{\rm b}$ — free-energy barrier for dissociation; $\tau_{\rm m}$ — aggregate lifetime; φ_2, φ_3—lower and upper bounds of the premicellar regime. A value of $\tau_0 = 10$ ns has been used for the molecular time scale.

Amphiphile	$m^{\min}(\varphi_2)$	$m^{\min}(\varphi_3)$	$F_{\rm b}(\varphi_2)$ $(k_{\rm B}T)$	$F_{\rm b}(\varphi_3)$ $(k_{\rm B}T)$	$\tau_{\rm m}(\varphi_2)$ (s)	$\tau_{\rm m}(\varphi_3)$ (s)
A	53	60	1.3	30.4	2.0×10^{-4}	1.3×10^{9}
B	118	128	0.5	112.5	4.3×10^{-2}	1.8×10^{43}

pendence of $\tau_{\rm m}$ on the barrier height (Eq. 3.19), which is the main source of concentration dependence. Two additional contributions to the dependence of $\tau_{\rm m}$ on ϕ are included in the prefactor of Eq. 3.19. The first, $(1 + F_s''(m^{\max})/2)^{-1}$, comes from the aggregation-number diffusion coefficient, $D(m)$. This factor is practically concentration-independent, since in our examples the curvature of the saddle point is small, $|F_s''(m^{\max})| < 0.1$, and thus $D(m^{\max}) \simeq (2\tau_0)^{-1} = \text{const}$. The second pre-exponential factor in Eq. 3.19, $|F_s''(m^{\min})F_s''(m^{\max})|^{-1/2}$, depends on concentration primarily through $|F_s''(m^{\max})|$, which is an increasing function of ϕ. This factor causes the slightly weaker increase of lifetime with ϕ at small concentration (Fig. 3.9).

In Fig. 3.9 we see that in the case of amphiphile A, assuming $\tau_0 \sim 10$ ns, the aggregate lifetime reaches the order of 1 s for $\phi \simeq 1.4\varphi_2$, whereas the cmc is at $\varphi_3 \simeq 2.75\varphi_2$. Thus, the premicellar aggregates remain stable for a macroscopic time over a significant part of the premicellar regime. In the case of amphiphile B we find $\tau_{\rm m} \sim 1$ s for $\phi \simeq 1.05\varphi_2$ while $\varphi_3 \simeq 4.2\varphi_2$, *i.e.*, the aggregates are kinetically stable over a much larger portion (practically all) of the premicellar concentration range, as expected for a much more hydrophobic amphiphile.

3.6 Discussion

Since micellization is evidently not a macroscopic phase separation, one should not expect the cmc to be a transition point [65]. Hence, existence of micelles at concentrations below the cmc, whatever the experimental definition of the cmc may be, is to be expected. The key question, therefore, relates to the extent and features of such premicellar aggregation. The formation of aggregates at $\phi < \phi^{\rm cmc}$, as arising from the

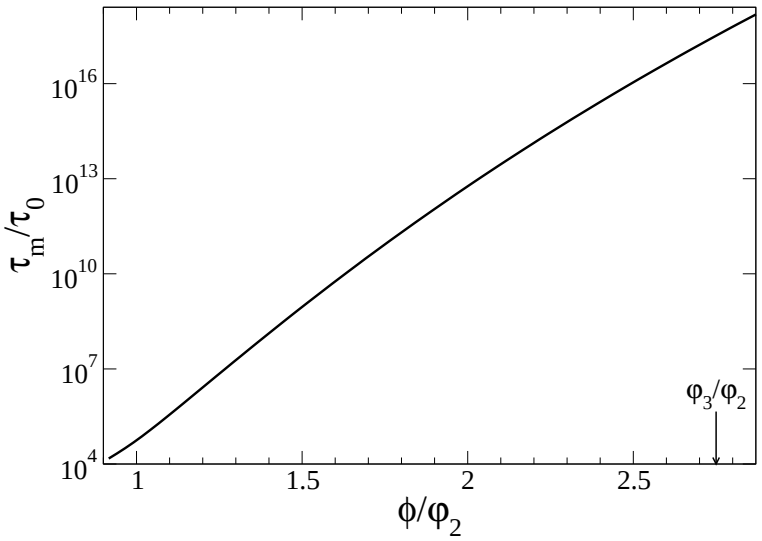

Figure 3.9: Lifetime of premicellar aggregates of amphiphile A as a function of amphiphile volume fraction. The lifetime is scaled by the molecular time scale τ_0 (of typical order of 10 ns), and the volume fraction by φ_2, the onset of premicellar aggregation. The volume fraction corresponding to the cmc (φ_3) is indicated by an arrow. Parameters of amphiphile A are given in Table 3.1.

mere fact that the aggregation number m is finite, is captured by earlier mass-action models (e.g., [9, 61]), as well as our simple analysis in the case of fixed m (Sec. 3.2.1). We find, indeed, continuous micelle formation at all concentrations, yet the fraction of amphiphiles participating in micelles in the fixed-m case remains very small (smaller than $1/m$) below the cmc.

When the aggregation number is properly treated as a degree of freedom, we find a concentration range below the (commonly defined) cmc, in which the fraction of amphiphiles in aggregates may reach tens percent at equilibrium. This surprising extent of premicellar aggregation, which is much larger than the one expected from mere finite-size effects (i.e., much larger than $1/m$), is one of our main results. It evidently depends on the fact that the system is free to choose the micelle size. We have shown that this freedom leads to a metastable aggregated state, containing monomers and aggregates, whose free energy per molecule differs little (in terms of $k_{\mathrm{B}}T$) from that of the pure monomeric state (see Fig. 3.2), and is thus significantly occupied at equilibrium. In addition, we have found that the favorable aggregate size changes only slightly in the premicellar as well as the micellar regions. The large extent of

premicellar aggregation and the concentration-insensitive micelle size are in qualitative agreement with the experiment of Ref. [62].

The model yields a discontinuous transition at very low concentration, $\phi = \varphi_1$, below which there are no aggregates. This is most probably a consequence of our two-state simplification, and we expect the transition to disappear when micellar polydispersity at low concentrations is properly taken into account. Our focus in the current work, however, is not on this low concentration regime, $\phi < \varphi_2$, where the extent of aggregation is negligible and the aggregation number significantly changes with ϕ, but rather on the region of potentially appreciable premicellar aggregation, $\varphi_2 < \phi < \varphi_3$.

We have found narrow size distributions of premicellar aggregates, *i.e.*, micelles below the cmc should be only slightly more polydisperse than their counterparts above the cmc. (See Fig. 3.8.) This agrees with the monodispersity observed in the experiment [62]. Thus, polydispersity does not pose a problem for the applicability of premicellar aggregation.

It has been shown in Sec. 3.5.2 that considerations of aggregate lifetime can reduce the concentration range in which premicellar aggregates may be experimentally observable and technologically relevant, compared to the range determined from equilibrium considerations alone. In other words, the apparent concentration, above which an appreciable amount of metastable and long-lived micelles appears, may be higher than φ_2. We have demonstrated, nonetheless, that kinetic stability (*i.e.*, macroscopic lifetime) still exists in most of the premicellar region. The range of stability is wider the more hydrophobic the surfactant. These conclusions are in line with results presented in Ref. [36]. Although that study does not deal with premicellar aggregation, it has shown that the dissociation time of (block copolymer) micelles remains very large even below the cmc.

Our Kramers-like approach, as already mentioned in Sec. 3.5.1, relies on two assumptions, which are violated near the edges of the premicellar region. The first assumption, of a high free-energy barrier between the metastable and stable states, is valid in almost the entire region except close to the lower edge, φ_2, where the barrier may become of order $k_{\mathrm{B}}T$ only. (See Table 3.2.) The resulting short lifetimes, though not accurately accounted for by the theory, are of little interest. The second assumption, of a large free-energy difference between the two states, holds in nearly

the entire range as well, except very close to the upper edge, φ_3, where, by definition, the free-energy difference vanishes. The free-energy difference, in units of $k_{\mathrm{B}}T$, becomes large quickly as ϕ gets smaller than φ_3, since the considered mesoscopic subsystem of volume V_s contains a large number of molecules (mostly monomers). In addition, correction of the theory near φ_3 by considering a probability backflow from the monomeric to the aggregated state will only increase the stability of the latter. Therefore, the deficiencies of the theory at the edges of the premicellar region do not affect our main results.

The results just summarized concerning premicellar aggregation, nevertheless, should be affected in practice by kinetic barriers, as demonstrated in Sec. 3.3. In our typical examples the nucleation barrier for premicellar aggregation is much larger than $k_{\mathrm{B}}T$. This, assuming a pure solution undergoing homogeneous nucleation, should lead to inability to observe premicellar aggregation within the experimental time limits. As the favorable aggregate size increases, so do the critical nucleus and nucleation barrier for aggregate formation (Figs. 3.6 and 3.7). For large micelles, one can expect that the experimentally observed micellization will be determined by these kinetic rather than equilibrium considerations [36]. Consequently, for such large micelles, not only could premicellar aggregation become irrelevant, but the experimentally observed cmc might be higher than the binodal-like point determined from equilibrium considerations, φ_3. It should be borne in mind, however, that such kinetic limitations are relevant to sufficiently pure systems; the presence of a third component acting as a nucleation center will naturally lower the barrier and promote premicellar aggregation. Apart from such heterogeneous nucleation, it might be possible to overcome large nucleation barriers within reasonable time scales by external means (*e.g.*, agitation or sonication).

The analysis presented in this chapter, in fact, suggests a possible simple resolution for the long-standing controversy regarding premicellar aggregation. Although the phenomenon should exist in fully equilibrated surfactant solutions (Sec. 3.2), it should be kinetically hindered in pure, unagitated systems (Sec. 3.3). This may explain why premicelles have been observed in solutions containing a very small quantity of an amphiphilic impurity (e.g., in fluorescence correlation and spectroscopy experiments involving amphiphilic probes [7]; Chapter 6, [62], [67], [68]) and not in pure solutions (e.g., using sensitive conductivity measurements [4], [11]). We shall return to this

point in Chapter 5.

Chapter 4

Kinetics of Surfactant Micellization

In this chapter we present another major application of the free-energy formalism, which was presented in Chapter 2. Here it is applied to the study of the kinetics of micelle formation and growth.[1]

4.1 Introduction

As already mentioned in Sec. 1.4, previous theories of the kinetics of surfactant micellization cast the process in the form of reaction kinetics with two separated time scales, whereby micelles form and disintegrate through a series of single monomer-exchange reactions. In this chapter we present an alternative approach, which is based on the free-energy formalism derived in Chapter 2. A similar strategy was previously applied to the kinetics of surfactant adsorption at interfaces [69, 70]. This approach has two main advantages. The first is that it provides a more unified description of the kinetics — rather than considering different stages as separate processes ("reactions"), they can all be examined as constrained pathways on a single free-energy landscape. Considering different processes on the same footing allows, for example, easier identification of rate-limiting stages such as diffusion-limited or kinetically limited ones [70]. The second advantage of such a formalism is that it can be more easily extended to more complex situations, e.g., ionic solutions or surfactant mixtures. The shortcoming

[1]The material presented in this chapter is being prepared for publication as Hadgiivanova, R.; Diamant, H.; Andelman, D. *Kinetics of Surfactant Micellization*, to be submitted to J. Phys. Chem. B.

of the model is that it is phenomenological, following coarse-grained thermodynamic variables rather than single molecules and aggregates. It is probably not appropriate for large polymeric micelles, where intramolecular degrees of freedom play an important role and a more detailed description of molecules and aggregates is required [39, 42, 43]. We shall focus here, therefore, on the micellization of small surfactants.

Another consequence of the coarse-grained modeling is that the derivation bears similarities to the kinetics of first-order phase transitions (See Sec. 1.6). (This is not the first time that such an analogy is invoked [38, 42].) However, unlike macroscopic phase separation, micellization is restricted to finite-size aggregates, resulting, e.g., in growth laws that are not scale-free.

In Sec. 4.2 we present the implications of the free-energy formalism for the process of micelle formation. As in previous theories we subsequently separate the kinetics into stages of disparate time scales, during each of which a different set of constraints is imposed. The initial nucleation stage is considered in Sec. 4.3. Section 4.4 describes the subsequent growth of the micellar nuclei as they absorb additional monomers from the surrounding solution. Both options of kinetically limited and diffusion-limited growth are studied. In addition, the possible role played by long-distance diffusive transport is examined. In Sec. 4.5 the final relaxation toward equilibrium is addressed. The surfactant solution may be either closed, containing a fixed number of surfactant molecules, or open, i.e., in contact with a large reservoir which is at equilibrium. Whereas in equilibrium this distinction is immaterial, the kinetics are found to be strikingly different. Whenever necessary we shall address the cases of closed and open systems separately. Finally, in Sec. 4.6 we discuss the limitations of our analysis, summarize the conclusions, and indicate important experimental implications.

4.2 Model

We begin as before with the free energy, F (Eq. 2.2), and consider the possible pathways on the free-energy landscape, which lead from an initial state of the system to the equilibrium state. At equilibrium the amphiphilic solution is spatially uniform and is characterized by single mean values for the variables (e.g., ϕ_1 and m), which minimize F for a given ϕ. Out of equilibrium the values of variables may be position-dependent,

and the total free energy is given by spatial integration of the local free-energy density.[2]

In Chapter 3 we studied the metastable premicellar aggregates, which may appear at concentrations below the cmc, φ_3. In this chapter we shall focus on the ordinary micellization region, $\phi > \varphi_3$, where micelles are stable at equilibrium. It should be kept in mind, however, that in this region the monomeric and micellar states are separated by a free-energy barrier in the form of a saddle point of F at $[\phi_1^{\min}(m^{\max}, \phi), m^{\max}, \phi]$. The barrier may be high, leading to the measurement of an apparent cmc, which is higher than the equilibrium one, φ_3 [36]. As already noted in Chapter 2, above a certain higher volume fraction, $\phi > \varphi_4 > \varphi_3$, the barrier disappears and the micellar state remains the sole minimum of F.

The initial and final states of the micellization kinetics are defined as follows. At $t = 0$ the system is in the monomeric state, $(\phi_1 = \phi, m = 1)$, whereas its equilibrium state is the micellar one. In a closed system this is done by setting the surfactant volume fraction above the cmc, $\phi > \varphi_3$ (using, e.g., a stopped-flow technique). In an open system the initial condition corresponds to opening a diffusive contact with a bulk reservoir, whose surfactant volume fraction is above the cmc, $\phi_{\rm b} > \varphi_3$, and which has already reached the equilibrium micellar state. At $t \to \infty$ the system reaches the global minimum of the free energy — $[\phi_1^{\min}(m^{\min}, \phi), m^{\min}(\phi), \phi]$ in the closed case and $[\phi_1^{\min}(m^{\min}, \phi_{\rm b}), m^{\min}(\phi_{\rm b}), \phi_{\rm b}]$ in the open one. In what follows we consider the kinetic pathway that the system takes between those initial and final states. Assuming separation of time scales, we shall break the path into separate stages. The various time scales, however, all derive from the free energy functional and a molecular time scale, thus enabling comparison of the different stages on the same footing.

Throughout the following sections we shall demonstrate the results using a single exemplary surfactant, whose parameters and properties are listed in Table 4.1. This allows comparison with Chapter 3, where the behavior of the same surfactant (Table 3.1) for $\phi < \varphi_3$ was presented.

Figure 4.1 shows two cuts through the free-energy landscape as a function of aggregation number for the exemplary surfactant in a closed system. Along the first cut (solid line) the monomer volume fraction is assumed to be at quasi-equilibrium,

[2] We neglect here surface-tension (gradient) terms associated with boundaries between such spatial domains.

Table 4.1: Parameters and properties of the exemplary surfactant

n	u_0	σ	κ	φ_3	φ_4
13	10	11	0.08	0.002028	0.1064

$\phi_1 = \phi_1^{\min}(m)$. Thus, the minimum of this curve corresponds to the global minimum — the equilibrium aggregation number. Along the other cut (dashed curve), which is relevant to the next two sections, we constrain the concentration of micelles to remain at its nucleation value.

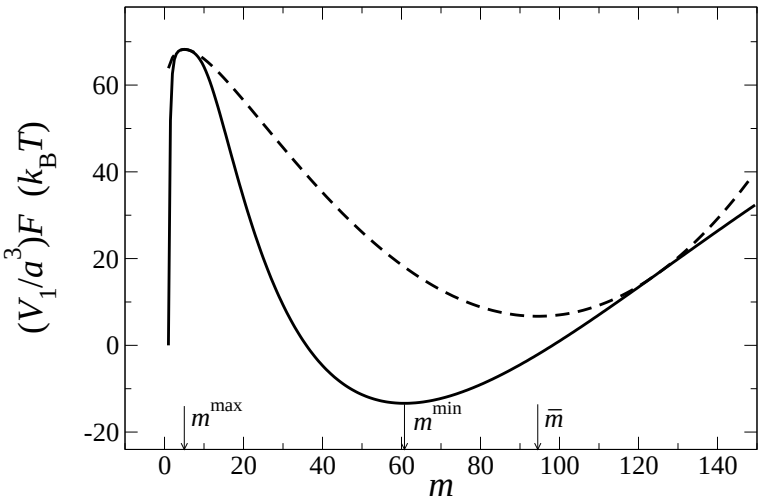

Figure 4.1: Cuts of the free energy landscape as a function of aggregation number for the surfactant parameters of Table 4.1 and $\phi = 1.1\varphi_3$. The two curves correspond to two different constraints: relaxation of the monomer volume fraction for the given aggregation number (solid), or fixed concentration of micelles (dashed). A closed system is assumed.

4.3 Nucleation

4.3.1 Closed system

For a closed system the total volume fraction at $t = 0$ is set to some value, $\phi > \varphi_3$, and (apart from a short initial period of homogenization which we ignore) that value remains fixed and uniform throughout the micellization process. The first stage to consider is the climbing from the initial metastable state, $(\phi_1 = \phi, m = 1, \phi)$, up the

free energy to the saddle point $[\phi_1 = \phi_1^{\min}(m^{\max}), m = m^{\max}, \phi]$, i.e., the formation of the critical nuclei (See Fig. 4.1). This activated process is assumed much slower than diffusion. Hence, ϕ_1 can be taken during this stage as spatially uniform and equal to the value that minimizes the free energy for the given ϕ and $m(t)$. Thus, as $m(t)$ increases from 1 to the critical-nucleus size $m^{\max}$, the system proceeds along the path that satisfies the constraints $\phi = \text{const}$ and $\phi_1 = \phi_1^{\min}[m(t), \phi]$.

A similar path was studied in detail in Chapter 3 to obtain the lifetime of metastable micelles in the region $\varphi_2 < \phi < \varphi_3$. Such a rigorous calculation, unfortunately, cannot be repeated here, since the metastable monomeric state is actually not a local minimum of F but just a cutoff at $m = 1$ (See Fig. 4.1). Nevertheless, as demonstrated in Sec. 3.5, the activation time (dissociation time in Sec. 3.5 and nucleation time in the current case) and its concentration dependence are primarily determined by the free-energy barrier.

Since our model does not explicitly consider single micelles but macrostates containing both micelles and monomers, we need to treat single-aggregate properties in an appropriate way. We do so using the arguments presented in Sec. 2.3. The relevant subsystem volume, V_s, is here the one that contains (on average) a single nucleus. The volume fraction of critical nuclei, their concentration, and the volume per nucleus are readily given by

$$\begin{aligned} \text{closed system:} \quad \phi_{\text{nuc}}(\phi) &= \phi - \phi_1^{\min}[m^{\max}(\phi), \phi] \\ c_{\text{nuc}}(\phi) &= \phi_{\text{nuc}}(\phi)/[na^3 m^{\max}(\phi)] \\ V_s(\phi) &= c_{\text{nuc}}^{-1} = \frac{na^3 m^{\max}(\phi)}{\phi - \phi_1^{\min}[m^{\max}(\phi), \phi]} \end{aligned} \tag{4.1}$$

Since ϕ_{nuc} is very small, V_s is much larger than the molecular volume, and our coarse-grained approach is indeed applicable. The nucleation barrier and nucleation time scale are given then by

$$\begin{aligned} \text{closed system:} \quad \Delta F_{\text{nuc}}(\phi) &= \frac{V_s(\phi)}{a^3}\left\{F[\phi_1^{\min}(m^{\max}, \phi), m^{\max}, \phi] - F_1(\phi)\right\} \\ \tau_{\text{nuc}}(\phi) &\sim \tau_0 e^{\Delta F_{\text{nuc}}(\phi)}, \end{aligned} \tag{4.2}$$

where F_1 is the free energy of the monomeric state (See footnote 3 in Sec. 3.2.2.) and

τ_0 a molecular time scale.

Various features of the nucleation stage can be calculated from Eqs. 2.2–2.5, 4.1 and 4.2, as demonstrated in Figs. 4.2–4.4. The concentration of critical nuclei (Fig. 4.2A) sharply increases with surfactant volume fraction as ϕ is increased above φ_3. The size of the critical nucleus (Fig. 4.3A) decreases with ϕ until it practically vanishes as ϕ approaches φ_4. The height of the nucleation barrier (Fig. 4.4) decreases as well with ϕ, leading to a sharp decrease in the nucleation time scale (Fig. 4.4 inset). To get an estimate of the actual nucleation time scales we may take $\tau_0 \sim 10$ ns (the time it takes a molecule with a diffusion coefficient $\sim 10^{-6}$ cm^2/s to be displaced by ~ 1 nm). For the example presented in Fig. 4.4 $\tau_{\rm nuc}$ is extremely large close to φ_3 but drops to ~ 1 s for $\phi \simeq 2\varphi_3$.

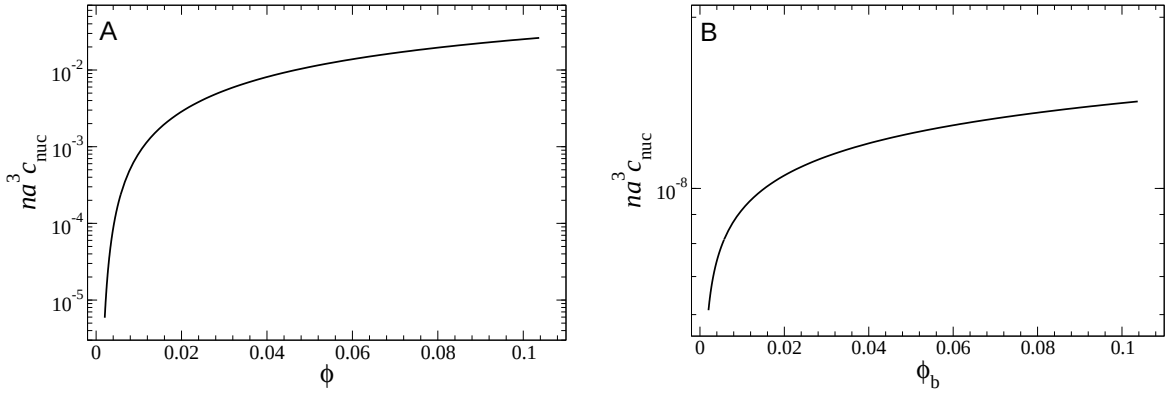

Figure 4.2: Concentration of critical nuclei (normalized by the molecular volume) as a function of surfactant volume fraction in the range between φ_3 and φ_4 for a closed (A) and open (B) systems. Parameters are given in Table 4.1.

4.3.2 Open system

When the system makes contact with an equilibrium reservoir of a higher volume fraction, $\phi_{\rm b} > \varphi_3$, monomers will first diffuse in, until the monomeric concentrations are balanced. We shall assume that micellar diffusion from the reservoir is either blocked or very slow. (If it is not, micellization in the system will be dominated by simple transport of micelles from the reservoir.) Thus, the starting point for the nucleation stage in this case is different from that of a closed system — it is still a monomeric state, yet with a lower volume fraction, $\phi_1 = \phi = \phi_{1\rm b} < \phi_{\rm b}$. Nucleation

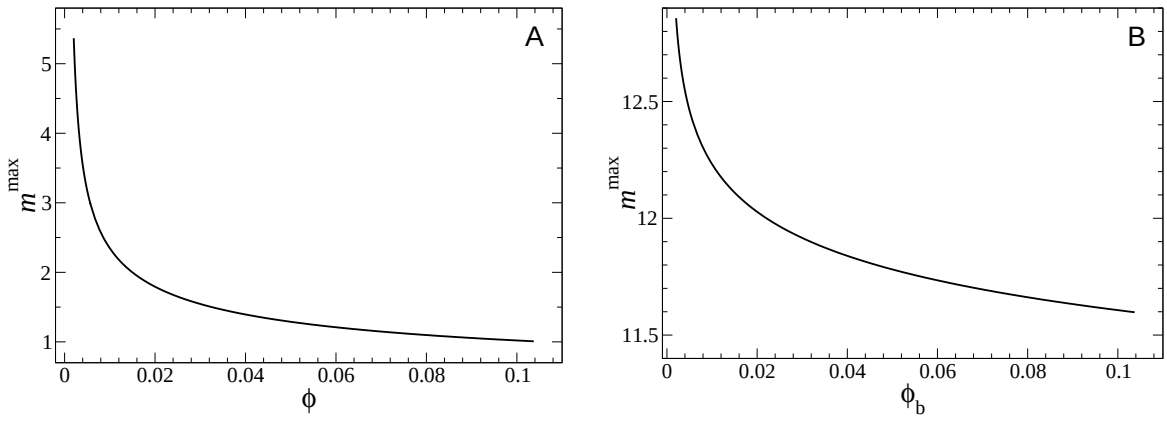

Figure 4.3: Critical-nucleus size as a function of surfactant volume fraction in the range between φ_3 and φ_4 for a closed (A) and open (B) systems. Parameters are given in Table 4.1.

is again assumed much slower than monomer diffusion. Hence, the monomer volume fraction remains fixed at $\phi_1 = \phi_{1\mathrm{b}}$. At the same time it should minimize F for the given $m(t)$, which determines the value of the third state variable, ϕ. As the nuclei grow, the total volume fraction increases, and the system proceeds along the path that satisfies the constraints $\phi_1 = \phi_1^{\min}[m(t), \phi] = \phi_{1\mathrm{b}}$.

The nucleation path ends at the state of critical nuclei, which is also different from the closed-system saddle point, because the total volume fraction has not reached the bulk value, $\phi < \phi_{\mathrm{b}}$. This state is given by the following set of equations:

$$\begin{aligned}
\text{open system:}\quad \phi_1^{\min}[m^{\max}(\phi), \phi] &= \phi_{1\mathrm{b}}(\phi_{\mathrm{b}}) = \phi_1^{\min}[m^{\min}(\phi_{\mathrm{b}}), \phi_{\mathrm{b}}] \\
&\Rightarrow \quad \phi = \phi(\phi_{\mathrm{b}}) \Rightarrow m^{\max} = m^{\max}(\phi_{\mathrm{b}}) \\
\phi_{\mathrm{nuc}}(\phi_{\mathrm{b}}) &= \phi - \phi_{1\mathrm{b}} \\
c_{\mathrm{nuc}}(\phi_{\mathrm{b}}) &= \phi_{\mathrm{nuc}}/(na^3 m^{\max}) \\
V_s(\phi_{\mathrm{b}}) &= c_{\mathrm{nuc}}^{-1} = \frac{na^3 m^{\max}(\phi_{\mathrm{b}})}{\phi(\phi_{\mathrm{b}}) - \phi_{1\mathrm{b}}(\phi_{\mathrm{b}})}.
\end{aligned} \tag{4.3}$$

The nucleation barrier and time scale are given then by

$$\begin{aligned}
\text{open system:}\quad \Delta F_{\mathrm{nuc}}(\phi_{\mathrm{b}}) &= \frac{V_s}{a^3}\left[F(\phi_{1\mathrm{b}}, m^{\max}, \phi) - F_1(\phi_{1\mathrm{b}})\right] \\
\tau_{\mathrm{nuc}}(\phi_{\mathrm{b}}) &\sim \tau_0 e^{\Delta F_{\mathrm{nuc}}(\phi_{\mathrm{b}})},
\end{aligned} \tag{4.4}$$

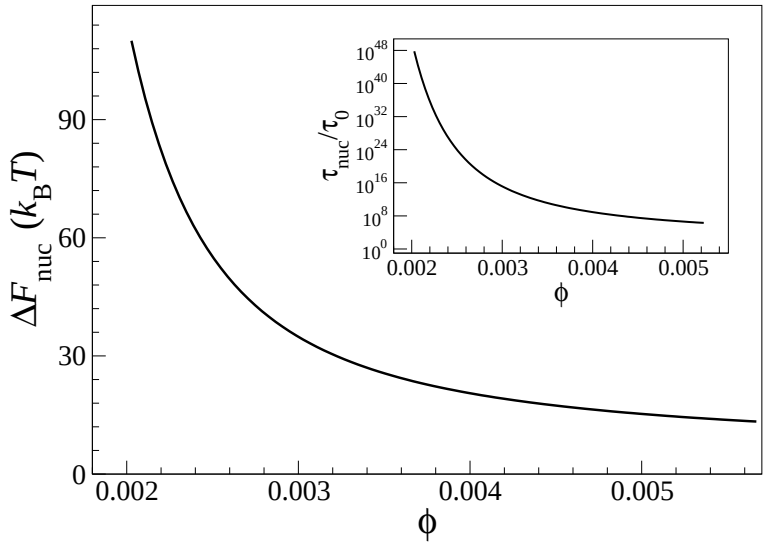

Figure 4.4: Nucleation barrier (in units of $k_{\rm B}T$) as a function of surfactant volume fraction for a closed system. The inset shows the corresponding nucleation time in terms of the molecular time scale τ_0. Parameters are given in Table 4.1.

where ϕ and $m^{\rm max}$ as functions of $\phi_{\rm b}$ are given by Eq. 4.3.

From Eqs. 2.2–2.5, 4.3, and 4.4 one can calculate the various parameters of the nucleation stage for an open system. Examples are shown in Figs. 4.2B and 4.3B, revealing striking differences from the case of a closed system. The explanation is straightforward — the system is assumed to be in contact with the reservoir only through its monomeric concentration, $\phi_{\rm 1b}$, which hardly changes as $\phi_{\rm b}$ is increased above the cmc. Hence, during this initial stage ϕ_1 remains low regardless of the value of $\phi_{\rm b}$. Consequently, the critical nuclei remain relatively rare and large, almost independent of concentration (Figs. 4.2B and 4.3B). Moreover, since ϕ_1 does not reach values above φ_3, we get very high nucleation barriers, resulting in an unphysical nucleation time for the open system. Thus, homogeneous nucleation in an open system, which does not have micellar transport from the reservoir, is strongly hindered. In the following discussion of open systems we shall assume that, despite this strong kinetic limitation, nuclei were somehow caused to form (e.g., through heterogeneous nucleation).

4.4 Growth

The nucleation stage addressed in Sec. 4.3 ends when the critical nuclei have formed. On the free-energy landscape the system has reached the saddle point of F. Subsequently, a stage of faster growth takes place, as the system rolls down the free energy toward larger m, the nuclei thereby absorbing additional monomers from the surrounding solution (cf. Fig. 4.1).

The growth is assumed much faster than the nucleation of new micelles or fusion and fission of existing ones. Hence, the concentration of micelles, $c_m = (\phi - \phi_1)/(na^3 m)$ remains fixed at $c_m = c_{\rm nuc}$. Consequently, the available volume per aggregate, V_s, remains unchanged as well. We shall assume that the growth is also faster than the diffusive transports among the aggregates (for closed and open systems) and with the reservoir (open system). The increase in m, therefore, comes solely at the expense of a decrease in the number of the surrounding monomers, while the total surfactant volume fraction is conserved. Thus, we describe the growth kinetics as a constrained path, $[\phi_1(t), m(t)]$, such that $c_m = c_{\rm nuc} = \text{const}$ and $\phi = \text{const}$.

Although diffusive transport into or out of the subsystem (of volume V_s) is assumed negligible during this stage, it is *a priori* unclear whether the growth process itself, within V_s, should be kinetically limited or diffusion-limited. We shall therefore examine both options below. The constraints and the equations derived in this section apply as well to closed and open systems, yet the values substituted for ϕ and $c_{\rm nuc}$ differ substantially. While for a closed system ϕ is the experimentally controlled surfactant volume fraction, for an open system ϕ gets the lower and weakly changing values determined from $\phi_{\rm b}$ according to Eq. 4.3. The concentration of nuclei is also much lower in the open-system case (cf. Fig. 4.2). Consequently, the results for the two cases are quite different.

The aforementioned constraints imply that the average monomer volume fraction decreases linearly with aggregation number,

$$\phi_1(t) = \phi - na^3 c_{\rm nuc} m(t). \tag{4.5}$$

We are left with one independent variable, $m(t)$, whose change in time could be

either kinetically controlled or diffusion-controlled. Yet, before studying the detailed evolution, let us examine its final state, which is common to both limits.

The final state of the growth stage, denoted $(\bar{\phi_1}, \bar{m})$, is given by the minimum of F along the constrained path, $(\partial F/\partial m)_{c_m=c_{\rm nuc},\phi=\rm const} = 0$. This yields

$$m = \bar{m}: \quad \ln[\phi_1(m)] + u(m) + mu'(m) + 1 - 1/m = 0, \tag{4.6}$$

where $\phi_1(m)$ is given by Eq. 4.5, and, once $\bar{m}$ is calculated, $\bar{\phi_1} = \phi_1(\bar{m})$. The resulting aggregation numbers and their dependence on the controlled surfactant volume fraction are presented in Fig. 4.5. Note that the aggregation number at the end of the current stage is not equal to the equilibrium micellar size, since it corresponds to a minimum of F along the constrained path rather than its global minimum. Unlike the equilibrium size, $m^{\rm min}$, which is bound by thermodynamic stability to increase with surfactant volume fraction (dotted lines in Fig. 4.5), the intermediate size $\bar{m}$ can have a richer behavior. Examined over a wider range of ϕ, $\bar{m}$ is found to be non-monotonous, having a maximum at $\phi < \varphi_3$. Hence, for the closed system it decreases with ϕ (Fig. 4.5A), whereas for the open system, which remains dilute throughout this stage, it increases with ϕ (and, therefore, with $\phi_{\rm b}$; Fig. 4.5B). In the closed system the growth overshoots the equilibrium size for $\phi \gtrsim \varphi_3$ and undershoots it at higher values. Whether $\bar{m}$ is larger or smaller than $m^{\rm min}$ is in accord with the question of whether $c_{\rm nuc}$ is smaller or larger than the equilibrium micellar concentration, respectively. (We shall return to this point when we deal with the final relaxation in Sec. 4.5.) In the open system $\bar{m}$ is very close to, and slightly smaller than, $m^{\rm min}$. Similar observations can be made concerning the final monomer volume fraction, $\bar{\phi_1}$, as demonstrated in Fig. 4.6.

We now turn to the evolution of the micellar size. We shall first assume, in Sec. 4.4.1, that it is kinetically limited. We will subsequently check in Sec. 4.4.2 whether such a description is consistent with the rate of monomer diffusion and consider the alternative of a diffusive growth.

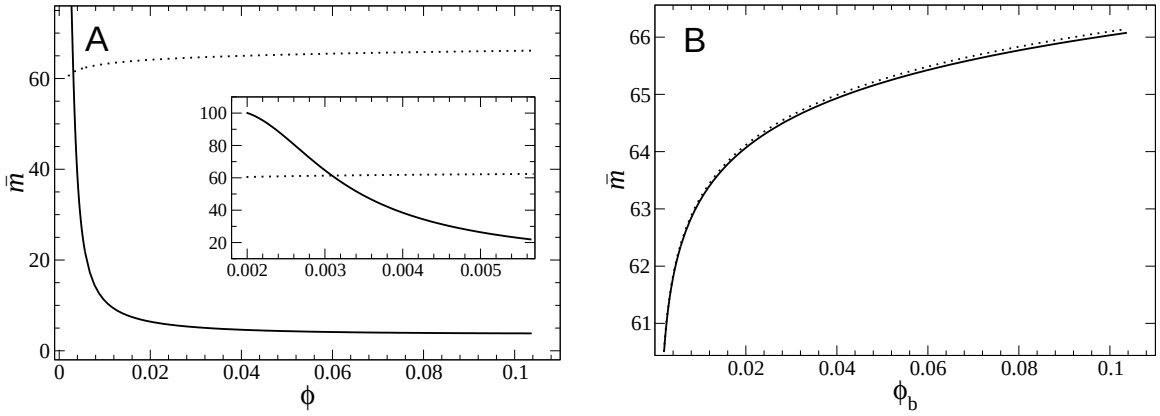

Figure 4.5: Intermediate micelle size at the end of the growth stage as a function of surfactant volume fraction in the range between φ_3 and φ_4 for a closed (A) and open (B) systems. The inset in A focuses on volume fractions slightly above φ_3. Dotted lines show for comparison the equilibrium micelle size, $m^{\min}$. Parameters are given in Table 4.1.

4.4.1 Kinetically-limited growth

In the case of kinetically limited growth the diffusive transport of molecules to the aggregate is assumed sufficiently fast so as not to limit the growth. The volume fraction of monomers, ϕ_1, satisfies Eq. 4.5 while being uniform across the sub-volume V_s. The increase of m with time is taken as proportional to the relevant thermodynamic driving force (i.e., the slope of F along the constrained path),

$$\frac{dm}{dt} = -\frac{\alpha}{\tau_0}\frac{V_s}{a^3}\left(\frac{\delta F}{\delta m}\right)_{\substack{c_m=c_{\rm nuc}\\ \phi=\text{const}}} = \frac{\alpha}{\tau_0}\left\{\ln[\phi_1(m)] + u(m) + mu'(m) + 1 - 1/m\right\}, \tag{4.7}$$

where α is a dimensionless prefactor, and $\phi_1(m)$ is given by Eq. 4.5. Equation 4.7, supplemented by a proper initial condition for $m(t=0)$, forms a simple initial-value problem for the temporal increase in micelle size, which can be solved numerically. Since the initial state of this stage is a stationary (saddle) point of F, we cannot begin with the strict initial condition, $m(0) = m^{\max}$, but have to perturb it to start the evolution.

An example for a numerical solution of Eq. 4.7, where we have taken $m(0) = m^{\max} + 1$ and $\phi = 1.1\varphi_3$, is shown in Fig. 4.7. The time scale of the growth, denoted

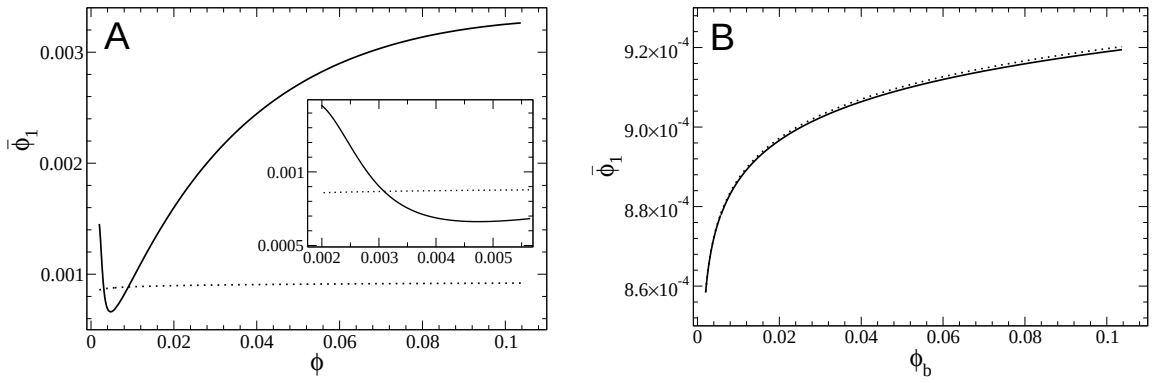

Figure 4.6: Monomer volume fraction at the end of the growth stage as a function of surfactant volume fraction in the range between φ_3 and φ_4 for a closed (A) and open (B) systems. The inset in A focuses on low volume fractions slightly above φ_3. Dotted lines show for comparison the equilibrium monomer volume fraction, $\phi_1^{\min}$. Parameters are given in Table 4.1.

$\tau_{\rm kin}$, is found to be about two orders of magnitude larger than the molecular time τ_0 (say, of order μs in this example).

To get an expression for the kinetic time scale we examine the asymptotic behavior of Eq. 4.7 as m approaches $\bar{m}$, obtaining

$$\begin{aligned} &\bar{m} - m(t) \sim e^{-t/\tau_{\rm kin}}, \\ &\tau_{\rm kin}^{-1} = \frac{\alpha}{\tau_0}\left[\frac{\phi-\phi_1}{m\phi_1} - 2u'(m) - mu''(m) - 1/m^2\right]_{m=\bar{m},\phi_1=\bar{\phi_1}}. \end{aligned} \tag{4.8}$$

The results for $\tau_{\rm kin}$ in terms of the molecular time τ_0 are shown in Fig. 4.8. For the closed system, over one decade of surfactant volume fraction, $\tau_{\rm kin}$ decreases from $\sim 10^2\tau_0$ to $\sim \tau_0$. (Values below τ_0, evidently, should not be regarded as physical.) The inset shows that the growth rate for the closed system increases roughly linearly with ϕ. For the open system the time scale is also about two orders of magnitude larger than τ_0, yet its dependence on $\phi_{\rm b}$ is much weaker for the reasons described in Sec. 4.3.2.

4.4.2 Diffusion-limited growth

In Sec. 4.4.1 we have assumed that the surrounding solution can supply the amount of monomers required for micellar growth within the time scale $\tau_{\rm kin}$. Let us check whether

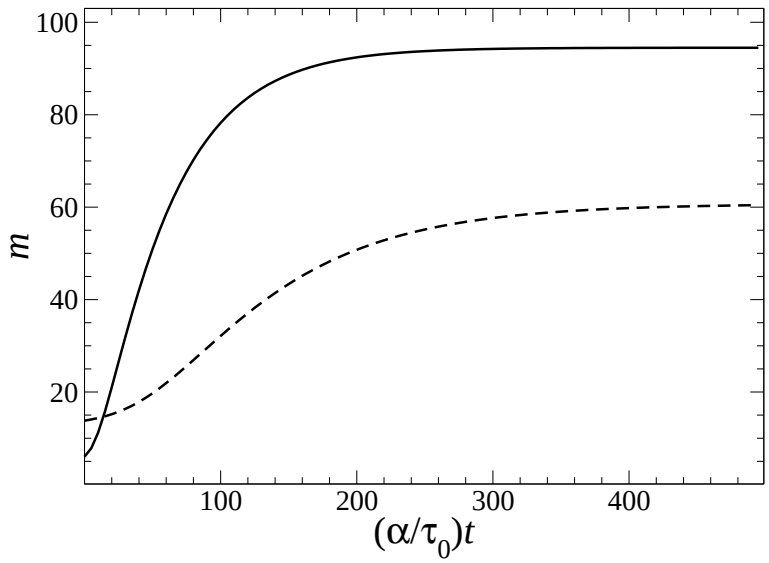

Figure 4.7: Temporal increase in micellar size assuming kinetically limited growth in a closed (solid line) and open (dashed line) system. The curves are obtained from numerical solution of Eq. 4.7 for the example of Table 4.1 and $\phi(\phi_b) = 0.00223 = 1.1\varphi_3$ for the closed (open) system.

this assumption is consistent with the rate of diffusive transport from the solution into the aggregate. The thickness of the diffusion layer around the aggregate, l_{dif}, satisfies the equation $\Delta m = (4\pi/3) l_{dif}^3 c_1$, where $\Delta m = (\bar{m} - m^{max})$ is the number of monomers to be transported and $c_1 = \phi_1/(na^3)$ the monomer concentration. The diffusion time scale is then $\tau_{dif} \sim l_{dif}^2/D$, D being the diffusion coefficient of a monomer. Using the definition $\tau_0 \sim (na)^2/D$ (i.e., τ_0 defined as the time it takes a molecule to diffuse along a distance comparable to its length), we obtain

$$\tau_{dif}/\tau_0 \sim [3\Delta m/(4\pi n^2)]^{2/3} \phi_1^{-2/3} \sim (0.1\text{–}1)\phi_1^{-2/3}, \tag{4.9}$$

where in the last relation we have assumed $n \sim 10$ and $\Delta m \sim 50$. For our typical example of $\phi_1 \sim 10^{-3}$ (cf. Fig. 4.5), $\tau_{dif} \sim (10\text{–}10^2)\tau_0$, i.e., comparable to τ_{kin}. Thus, the situation concerning the limiting process for micelle growth is not clearcut, and both processes may be relevant in general.

To treat the diffusion-limited growth in more detail we employ the following approximations. First, we neglect the increase in the micellar radius, R, and take it as constant. Although this description is evidently inaccurate, it crucially allows us to

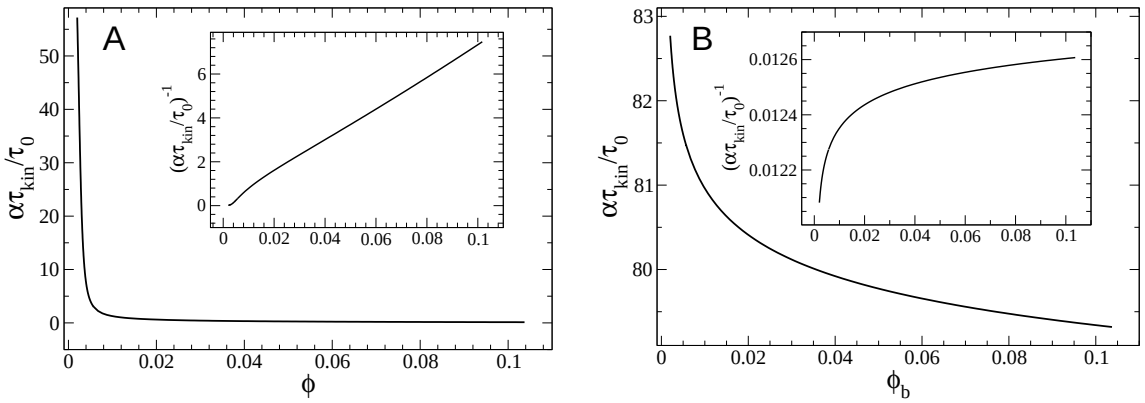

Figure 4.8: Time scale of kinetically limited growth as a function of surfactant volume fraction in the range between φ_3 and φ_4 for a closed (A) and open (B) systems. The insets show the increase of $\tau_{\rm kin}^{-1}$ (growth rate) with ϕ or $\phi_{\rm b}$. Parameters are given in Table 4.1.

avoid the complicated treatment of a moving boundary. Since the growth does not begin from a single monomer but from a critical nucleus of finite size $m^{\max}$, we do not expect the approximation of constant R to qualitatively affect the results. Second, the diffusion layer is assumed much smaller than the subsystem, $l_{\rm dif} \ll V_s^{1/3}$, thus allowing us to consider the latter as infinite, and the monomer volume fraction far from the micelle as given by Eq. 4.5. Third, we neglect back flow (desorption) of monomers from the micelle to the solution. This is justified in view of the strong driving force (large slope of F) for growth above the critical nucleus.

We assume a radial volume-fraction profile of monomers, $\phi_1(r > R, t)$, which follows the diffusion equation,

$$\frac{\partial \phi_1}{\partial t} = D \frac{1}{r^2} \frac{\partial}{\partial r} \left(r^2 \frac{\partial \phi_1}{\partial r} \right). \tag{4.10}$$

The growth of a micelle is determined by the diffusive flux of monomers from the solution,

$$\frac{dm}{dt} = D \frac{4\pi R^2}{na^3} \left. \frac{\partial \phi_1}{\partial r} \right|_{r=R}. \tag{4.11}$$

The boundary condition far from the micelle is given according to Eq. 4.5 by

$$\phi_1(r \to \infty, t) = \phi - na^3 c_{\rm nuc} m(t). \tag{4.12}$$

For the problem to be well posed, Eqs. 4.10–4.12 should be supplemented by appropriate initial conditions for $\phi_1(r,0)$ and $m(0)$, as well as a local "adsorption isotherm" at the aggregate surface, relating $\phi_1(R,t)$ and $m(t)$. The latter lies beyond the scope of our coarse-grained description. At any rate, we are interested primarily in the qualitative asymptotics of the diffusive transport from the solution into the aggregate, for which these details are not crucial. The asymptotic behavior as the final state of the growth stage is approached is worked out in the Appendix, yielding

$$\phi_1(R, t \to \infty) \simeq \bar{\phi_1}\left[1 - (\tau_{\text{dif}}/t)^{3/2}\right], \quad \tau_{\text{dif}} = \frac{a^2(n\Delta m)^{2/3}}{4\pi D}\bar{\phi_1}^{-2/3}. \tag{4.13}$$

Thus, unlike the exponential relaxation of a kinetically limited process (Eq. 4.8), the diffusive relaxation is characterized by a slow power law. Upon substituting $\tau_0 \sim (na)^2/D$ in Eq. 4.13 the general form of τ_{dif}, derived earlier from heuristic arguments (Eq. 4.9), is confirmed. Figure 4.9 shows the dependence of τ_{dif} on the controlled surfactant volume fraction according to Eq. 4.13, where we have taken $\tau_0 = (na)^2/D$. The cases of closed and open systems are again found to behave qualitatively differently, τ_{dif} strongly decreasing with ϕ in the former and weakly increasing with ϕ_{b} in the latter. This is a consequence of the different dependencies of $\bar{m}$ on concentration, commented on earlier (cf. Fig. 4.5). Comparison of Figs. 4.8 and 4.9 confirms our earlier assessment, that τ_{kin} and τ_{dif} are comparable in general, and both growth mechanisms may be relevant. For a closed system at concentrations slightly above the cmc we get for our representative example $\tau_{\text{dif}} \gg \tau_{\text{kin}}$, i.e., strictly diffusion-limited growth. [3]

4.4.3 Role of bulk diffusion

In Sec. 4.4.2 we have considered the local diffusive transport that takes place around individual micelles, feeding them with monomers. In the case of an open system there should also be slower, long-distance diffusion of monomers from the bulk reservoir. In principle this should have been the next stage to consider. However, for an open

[3] Bear in mind that τ_{kin} and τ_{dif} are associated with very different time dependencies — an exponential law vs. a power law — and are defined only up to a numerical prefactor. Hence, they should be compared with respect to the order of magnitude only.

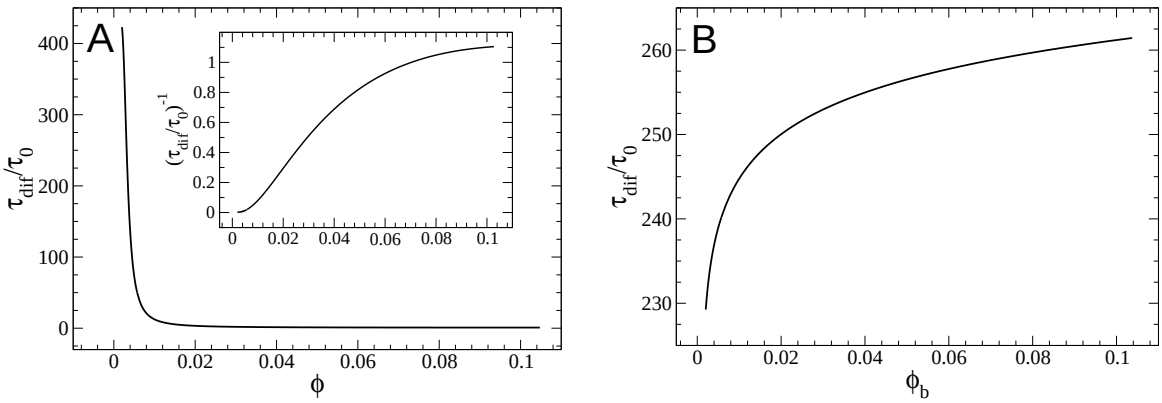

Figure 4.9: Time scale of diffusion-limited growth as a function of surfactant volume fraction in the range between φ_3 and φ_4 for a closed (A) and open (B) systems. Parameters are given in Table 4.1.

system we find that the monomer volume fraction at the end of the growth stage, $\bar{\phi}_1$, is invariably very close to the equilibrium (bulk) value, $\phi_1^{\min}$. (See Fig. 4.6B.) This is a consequence of the small number of initial nuclei (Fig. 4.2B), whose growth consumes, therefore, a small number of monomers. Thus, the driving force for bulk diffusion is very weak. Consistently, for an open system we find also that the micellar size at the end of the growth stage, $\bar{m}$, is very close to the equilibrium size, $m^{\min}$ (Fig. 4.5B). Therefore, at any rate, the bulk diffusion that does occur after the growth stage has a very minor contribution to the micellization.

4.5 Final relaxation

At the end of the growth stage monomer transport into the existing micelles has been exhausted, and the micelles have equilibrated with the surrounding monomers. Yet, the final state of this stage, $(\bar{\phi}_1, \bar{m})$, does not correspond to the global free-energy minimum, since up till now we have constrained the concentration of micelles to remain at its nucleation value (cf. Fig. 4.1). A slower process should ensue, therefore, during which the size and/or concentration of micelles relax to their equilibrium values.

In the open system the situation is a bit unusual. (Recall from Sec. 4.3, however, that actually reaching the current stage in an open system should already involve overcoming high barriers.) The monomer volume fraction has equilibrated with the

bulk reservoir and reached its equilibrium value. The size of the existing individual micelles has equilibrated as well, reaching $m^{\min}$. What has not equilibrated yet is the total surfactant volume fraction — specifically, the contribution to ϕ from the micellar concentration. Since there is no thermodynamic driving force for either monomer transport or changes in the size of the existing micelles, and we do not allow for transport of micelles from the reservoir, the only open pathway to final relaxation is the very slow nucleation of additional micelles. The newly formed micelles will take monomers from the solution, causing transport of additional monomers from the reservoir, until the total surfactant volume fraction reaches its equilibrium value, ϕ_{b}.

The relaxation of the closed system is qualitatively different. Both the monomer volume fraction and aggregation number have not equilibrated yet and will change in time while keeping the total surfactant volume fraction constant. We expect changes in the micellar concentration to occur through fusion or fission of micelles. Two additional processes, which in principle can be considered, are less relevant in this case. First, nucleation of new micelles or complete disintegration of existing ones might occur but will require the much longer time scale of τ_{nuc}. Second, Ostwald ripening — a common relaxation mechanism where larger domains grow at the expense of smaller ones — is not expected to take place, since the micelles are not unstable and the required positive feedback is thus lacking.

Either fission or fusion should be dominant, depending on whether $\bar{m}$ has overshot or undershot, respectively, the equilibrium size $m^{\min}$. (See Fig. 4.5A.) Correspondingly, the micellar concentration c_m will either increase or decrease, respectively, with time. Over the time scale of these rearrangements of aggregate size and concentration we can assume that the monomer volume fraction is relaxed, i.e., $\phi_1(t) = \phi_1^{\min}[m(t), \phi]$. We are left again with a single kinetic variable — either $m(t)$ or $c_m(t)$. The two are related via

$$c_m(t) = \{\phi - \phi_1^{\min}[m(t), \phi]\}/[na^3 m(t)]. \tag{4.14}$$

The kinetic equation for the micellar size reads

$$\begin{aligned} \frac{dm}{dt} &= -\frac{\beta}{\tau_m}\frac{V_s}{a^3}f(m) \\ f(m) &= \left(\frac{\delta F}{\delta m}\right)_{\substack{\phi_1=\phi_1^{\min}(m) \\ \phi=\text{const}}} = \\ &= \phi_1^{\min\prime}\ln\phi_1^{\min} - \left[\frac{\phi-\phi_1^{\min}}{m^2}+\frac{\phi_1^{\min\prime}}{m}\right]\ln(\phi-\phi_1^{\min}) \\ &\quad -(\phi-\phi_1^{\min})u'(m)+[u(m)+1-1/m]\phi_1^{\min\prime}, \end{aligned} \tag{4.15}$$

where $V_s = na^3 m^{\min}/[\phi - \phi_1^{\min}(m^{\min})]$ is here the volume per micelle at equilibrium, $\phi_1^{\min}(m)$ is given by Eq. 2.4, a prime denotes $\partial/\partial m$, and β is a dimensionless prefactor. We have introduced another microscopic time scale, τ_m, which characterizes the single-micelle dynamics. It is expected to be orders of magnitude larger than the molecular time τ_0 — either because of the long diffusion time required for two micelles to meet before fusing (in which case τ_m should be of order, say, 10^{-5}–10^{-4} s), or due to kinetic barriers for fusion or fission, which are not explicitly accounted for by our model.

Equations 2.4 and 4.15 can be solved numerically to obtain $m(t)$ and, subsequently (via Eq. 4.14), also $c_m(t)$. Figure 4.10 shows the solutions for our exemplary surfactant and two volume fractions, corresponding to fission- and fusion-dominated relaxation.

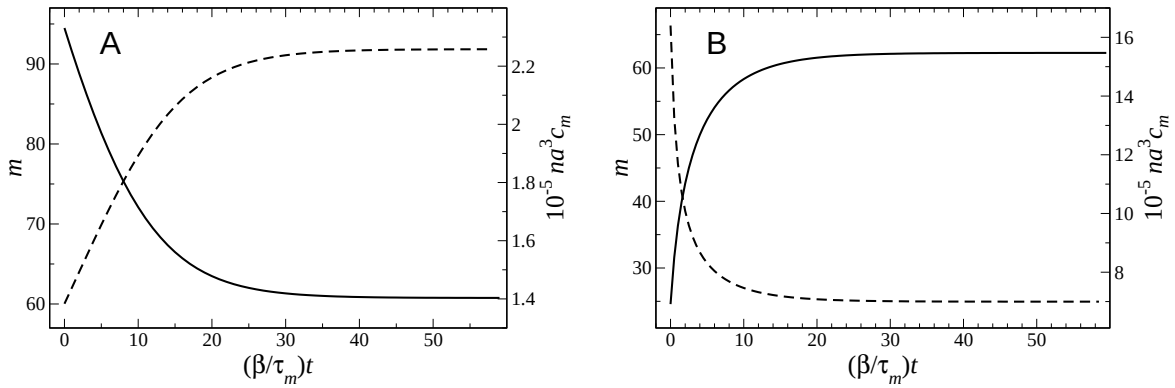

Figure 4.10: Evolution of micellar size (solid) and concentration (dashed) during the final relaxation stage in a closed system. Parameters are given in Table 4.1, and the volume fraction is $\phi = 0.00223 = 1.1\varphi_3$ (A) and $0.00523 = 2.58\varphi_3$ (B).

To find the relaxation time we examine the asymptotic behavior of $m(t \to \infty)$

according to Eq. 4.15, obtaining

$$|m(t) - m^{\min}| \sim e^{-t/\tau_{\rm rel}}$$
$$\tau_{\rm rel} = \frac{\tau_m}{\beta}\frac{a^3}{V_s}\frac{1}{f'(m^{\min})}, \tag{4.16}$$

where $f(m)$ has been defined in Eq. 4.15. The dependence of $\tau_{\rm rel}$ on surfactant volume fraction is shown in Fig. 4.11. The relaxation time is found to depend weakly on ϕ, remaining of the same order as (or slightly larger than) the single-micelle time τ_m throughout the concentration range.

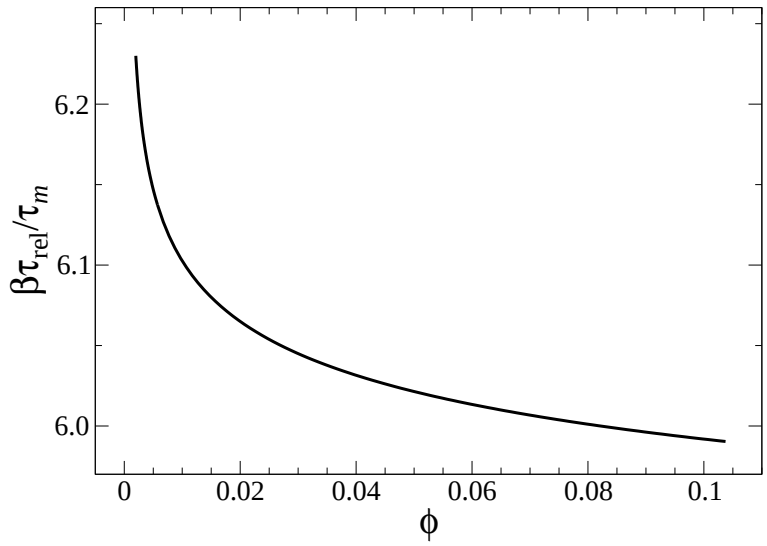

Figure 4.11: Time scale of final relaxation as a function of surfactant volume fraction in the range between φ_3 and φ_4 for a closed system. Parameters are given in Table 4.1.

4.6 Discussion

Our findings concerning the kinetics of micelle formation have several experimental implications. A particularly clearcut one relates to micellization in an open system — a solution in diffusive contact with a reservoir of monomers and micelles. We have found that, in cases where only monomer transport from the reservoir is allowed and the transport of micelles is blocked, micellization should be kinetically suppressed. The suppression is two-fold. First, strong activation is required for the homogeneous

nucleation of the first micelles (Sec. 4.3). This stems from the low surfactant concentration maintained in the system due to the correspondingly low monomer concentration (sometimes referred to as inter-micellar concentration) in the reservoir. Second, even after micelles do nucleate and grow, their final relaxation toward the equilibrium aggregation number and micellar concentration should be hindered, since the relaxation pathway requires the nucleation of additional micelles (Sec. 4.5). The consequent prediction is that the formation of micelles in such open monomeric solutions may be suppressed for a macroscopically long time. In fact, this behavior is regularly manifest in applications involving micelle-enhanced ultrafiltration [71]. It has also been observed in dialysis experiments [72], where the time scale of micelle formation was estimated as 1–10 hours. In ultrafiltration procedures and the dialysis experiment a micellar solution is forced through a membrane, whose pores are smaller than the micelles. The surfactant solution on the other side of the membrane remains monomeric for a macroscopically long time despite its contact with a micellar solution above the cmc.

We have analyzed the kinetics of micelle formation as divided into three major stages — nucleation, growth, and final relaxation of micellar size and concentration. This separation into distinct stages should be generally valid, as the corresponding three time scales are quite well separated. Such three stages have been resolved in a recent x-ray scattering experiment on block copolymer micellization [46]. They also emerged in other micellization theories [38].

The nucleation stage is much longer than all others and, since it is an activated process, its duration is exponentially sensitive to surfactant volume fraction as well as other parameters (Fig. 3.7). The range of nucleation times that we get for our exemplary surfactant in a closed system (typically larger than 1 s) is in line with measured values of $m\tau_2$ — the time scale for formation or disintegration of entire micelles [11]. The high nucleation barriers found close to the equilibrium cmc ($\phi = \varphi_3$) imply that the measured (apparent) cmc might in certain cases be higher than the equilibrium value. This issue, which was raised before in the context of block copolymer micelles [36], clearly merits further study.

The growth stage occurs on much faster time scales (e.g., 10^{-6}–10^{-5} s for our example). These time scales are similar to those measured for τ_1 — the single-monomer

exchange time at equilibrium [11]. We have found that the growth may in general be either diffusion- or kinetically limited, and that it should be diffusion-limited at concentrations close to the cmc. This is in accord with τ_1 being usually diffusion-limited for short-chain surfactants while becoming kinetically limited for longer-chain ones, which face higher kinetic barriers for incorporating into a micelle [11]. The diffusion-limited growth has a distinctive 3/2 power-law relaxation (Eq. 4.13), which should be verifiable in scattering experiments like the one described in Ref. [46], when they are applied to short-chain surfactants.

The final relaxation stage (in a closed system) may involve either reduction in aggregate size (fission), accompanied by an increase in aggregate concentration, or the other way around (fusion). (See Fig. 4.10.) Which of these scenarios holds depends on whether the aggregate size attained in the preceding growth stage has overshot or undershot the equilibrium aggregation number. The former should hold at concentrations close to the cmc, whereas the latter occurs at higher concentrations. We note that in the experiment of Ref. [46] the aggregates grew in size during their final relaxation, which is in line with the fact that the amphiphile concentration was much higher than the cmc. An interesting consequence of this analysis is that, by tuning to the right surfactant concentration, one should be able to eliminate the final-relaxation stage altogether, thus reaching the equilibrium micellar state already at the end of the growth stage. Another relevant prediction is that the relaxation time of this final stage should be almost independent of surfactant concentration (Fig. 4.11).

The main shortcoming of our model is its mean-field character. We have assumed that the kinetics in the surfactant solution can be described within a representative sub-volume, V_s, containing a single aggregate and being uncorrelated with the other sub-volumes. Upon closer inspection, in fact, we find that V_s for a closed system typically contains ~ 10–10^2 surfactant molecules, which is comparable to the aggregation number. Hence, correlations among such sub-volumes are to be expected as the micelles nucleate and grow. Another important mean-field aspect is our description of the state of the system as a deterministic point, and its kinetics as a sharply defined path, on the free-energy landscape. In practice, and particularly close to the cmc, the system should be more accurately described by stochastic distributions, with polydispersity and occupancies of both the monomeric and aggregated states [56]. (See Sec.

3.2.) Nonetheless, we do not expect these approximations to qualitative change our main results.

Chapter 5

Conclusions and Experimental Implications

The self-assembly of amphiphilic molecules into compact aggregates is an important process with numerous biological, technological, and scientific applications. The process also serves as a model system for the study of more complicated systems in soft matter physics and biology. In this thesis we have aimed to present simple theoretical models, which capture the well known as well as new qualitative features of micelle-forming systems in experimentally relevant scenarios.

The general free-energy formalism derived in Chapter 2 is a simple and powerful tool to study various problems concerning micellar aggregation. We have shown that, despite its simplicity, it enables one to approach nonequilibrium problems such as metastable aggregates and the kinetics of micelle growth from a new direction. Since it contains a minimum number of molecular parameters, it gives a general, unified description of the qualitative properties of micellar solutions.

In Chapter 3 we have characterized the phenomenon of premicellar aggregation and proposed an explanation as to why it has been so much disputed among scholars during the years. We have shown that, *at complete equilibrium*, a metastable aggregated state in an amphiphilic solution can be occupied to a large extent due to its small free-energy distance from the stable monomeric state. This highly occupied aggregated state is identified as the premicellar state. At the same time, we have shown that the nucleation barrier to the formation of premicellar aggregates can be very high,

especially in the case of larger micelles. This should lead in many cases to inability to observe homogeneously nucleated premicellar aggregates in the experiment's time limits. If the nucleation barrier is very high one may actually measure a cmc, which is higher than the equilibrium one (apparent cmc). Our analysis assumes, however, that the system is pure (i.e., consisting only of amphiphile and water). Even a very small amount of a third (hydrophobic or amphiphilic) component can act as a nucleation center, and thus effectively decrease the nucleation barrier and promote premicellar aggregation. This fact might explain why certain experiments observe premicellar aggregation while others do not, as the observation of premicellar aggregates likely depends on the method used. The strongest support for the existence of premicellar aggregation so far has come from spectroscopic methods, which require the addition of an amphiphilic fluorescent dye, which can act like such a heterogeneous-nucleation agent. No convincing support for premicellar aggregation has come, however, from macroscopic methods such as conductivity measurements, which do not introduce foreign agents and can be performed in highly purified solutions and with high sensitivity. Our analysis, therefore, suggests the following novel perspective on this controversial issue. Premicelles should exist in certain cases at equilibrium, yet their formation is kinetically hindered. The premicelles observed in some cases may be genuine, in the sense that the impurity present in such experiments does not lower the cmc for the formation of stable micelles, but rather facilitates the formation of (the otherwise kinetically hindered) metastable micelles.

To verify the predictions of Chapter 3 a number of measurements can be performed. To measure the size and polydispersity of the premicellar aggregates techniques like FCS were already shown to be applicable [62]. To measure the lifetime of the aggregates one can in principle apply methods like stopped-flow, where the concentration of micelles can be measured as a function of time upon dilution of the system, or use relaxation methods like ultrasonic spectroscopy [11, 73]. The possibility that in certain cases the apparent cmc, as measured experimentally, is affected by kinetic limitations and is not the true equilibrium cmc, clearly calls for further investigation and re-examination of published data. For example, such an apparent cmc should be accompanied by hysteresis effects upon re-dilution. Another "fingerprint" of a kinetically determined cmc might be found in the effect of a small concentration of a third

agent (impurity). When equilibrium is considered, one expects a smaller effect of a given concentration of impurity on shorter-chain surfactants, which have a higher cmc. If kinetics are concerned, on the other hand, the effect of impurity should be smaller on longer-chain surfactants, which have a higher nucleation barrier and a larger critical nucleus.

The theory of micelle formation and growth presented in Chapter 4 gives a unified picture of the process, since the different stages involved can be considered and compared using a single formalism. One of our main results is that, although the final equilibrium state of the open and closed system scenarios is the same, the kinetics of the two are strikingly different. In an open system, where the contact with a reservoir at concentration above the cmc is only through monomer exchange, the formation of micelles is expected to be suppressed, since it will proceed mainly through slow nucleation of new micelles. In the closed system we find that during the growth stage, where both diffusion and kinetic control may play a role, the size of the micelles either overshoots or undershoots the equilibrium micelle size depending on the amphiphile concentration. This stage is followed by relaxation processes of fission or fusion of micelles. Such a behavior has been observed in computer simulations [24].

The kinetic theory raises a number of suggestions for future experimental work. The scenarios of open and closed systems are experimentally achievable. Our findings of strongly suppressed micellization in an open system, if only diffusion of monomers from a reservoir is allowed, provide a theoretical explanation for a commonly encountered scenario in micelle-enhanced ultrafiltration procedures and are in agreement with a dialysis experiment [72]. Technical capability of following the formation of micelles in detail has been demonstrated recently [46, 74]. Such capabilities open new possibilities to examine the detailed predictions given in Chapter 4 — e.g., diffusion-limited vs. kinetically limited growth, overshoot in aggregate size, concentration dependencies, etc. The three stages of micellization, exhibiting different time scales, have been already observed for block copolymer micelles [46]. We hope that our results will motivate further studies for short-chain surfactants.

Overall, the free-energy formalism developed and used throughout this work has proved to be a useful tool for the study of micellization. Another interesting application may be the study of "spinodal micellization", where a deep initial quench (in

concentration or temperature) removes the nucleation barrier for micelle formation. We hope, therefore, that the theoretical framework and results presented here will lead to future theoretical and experimental studies. For example, our free-energy formalism allows for easy extensions of the theory to include additional effects and interactions, such as electrostatics and surfactant mixtures.

Appendix: Analysis of Diffusion-Limited Growth

In this appendix we calculate the asymptotic time dependence of the micellar size, $m(t)$, in a diffusion-limited growth. The equations to be handled are 4.10–4.12.

To leading order at long times we can substitute in Eq. 4.12 $m(t) \simeq \bar{m}$, turning the boundary condition far away from the micelle into $\phi_1(r \to \infty, t) = \bar{\phi_1}$. We now define $\psi(r,t) = \phi_1(r,t) - \bar{\phi_1}$, so that $\psi(r \to \infty, t) = 0$, and introduce Laplace-transformed variables, $\hat{\psi}(r,s) = \int_0^\infty dt e^{-st}\psi(r,t)$, $\hat{m}(s) = \int_0^\infty dt e^{-st} m(t)$. The diffusion equation, Eq. 4.10, is then rewritten as

$$s\hat{\psi} = D\frac{1}{r^2}\frac{\partial}{\partial r}\left(r^2\frac{\partial\hat{\psi}}{\partial r}\right), \tag{5.1}$$

(where we have assumed $\psi(r,0) = 0$, as the accurate initial profile should not affect the long-time asymptotics), and the boundary conditions, Eq. 4.11 and 4.12, transform to

$$s\hat{m} - m^{\max} = D\frac{4\pi R^2}{na^3}\left.\frac{d\hat{\psi}}{dr}\right|_{r=R} \tag{5.2}$$

$$\hat{\psi}(r \to \infty, t) = 0. \tag{5.3}$$

The solution of Eqs. 5.1–5.3 is

$$\hat{\psi}(r,s) = -\frac{na^3}{4\pi D}\frac{s\hat{m} - m^{\max}}{1 + R(s/D)^{1/2}}\frac{e^{-(s/D)^{1/2}(r-R)}}{r}, \tag{5.4}$$

from which we get

$$\hat{\psi}(R,s) = -\frac{na^3}{4\pi DR}\frac{s\hat{m} - m^{\max}}{1 + R(s/D)^{1/2}}. \tag{5.5}$$

The limit $t \to \infty$ corresponds to $s \to 0$, at which $s\hat{m} - m^{\max} \simeq \bar{m} - m^{\max} = \Delta m$. Subsequently inverting Eq. 5.5 back to real time and taking the limit $t \to \infty$, we find

$$\psi(R, t \to \infty) \simeq -\frac{na^3 \Delta m}{8(\pi D t)^{3/2}}, \tag{5.6}$$

which yields Eq. 4.13 for τ_{dif}.

Bibliography

[1] Tanford, C. *The Hydrophobic Effect: Formation of Micelles and Biological Membranes*, Krieger: Malabar, 1991.

[2] Israelachvili, J. *Intermolecular and Surface Forces*; 2nd Ed., Academic Press: London, 1992.

[3] F. Evans and H. Wennerström, *The Colloidal Domain*; 2nd Ed., Wiley: New York, 1999.

[4] Holmberg, K.; Jonsson, B.; Kronberg, B.; Lindman, B. *Surfactants and Polymers in Aqueous Solution*; 2nd Ed. Wiley and Sons Ltd: Chichester, 2002.

[5] Domb, C.; Lebowitz, J. L.; Gompper, G.; Schick, M. *Self-Assembling Amphiphilic Systems (Phase Transitions and Critical Phenomena*; Academic Press: London, 1994.

[6] Israelachvili, J.; Mitchell, J.; Ninham, B. W. *J. Chem. Soc. Faraday Trans.* **1976**, *72*, 1525–1568.

[7] Myers, D. *Surfactant Science and Technology*; 3rd Ed. Wiley and Sons Ltd: Hoboken, New Jersey, 2006.

[8] Patist, A.; Oh, S. G.; Leung, R.; Shah, D. O. *Coll. Surf. A* **2000**, *176*, 3–16.

[9] Lindman, B.; Wennerstrom H. *Micelles*, Springer-Verlag: Berlin, 1980.

[10] Yoshikiyo, M. *Micelles: Theoretical and Applied Aspects*, Plenum Press: New York, 1992.

[11] Zana, R., Ed. *Dynamics of Surfactant Self–Assemblies*; CRC Press: Boca Raton, FL, 2005.

[12] Tanford, C. *J. Phys. Chem.* **1974**, *78*, 2469–2479.

[13] Ruckenstein, E.; Nagarajan, R. *J. Phys. Chem.* **1975**, *79*, 2622–2626.

[14] Nagarajan, R.; Ruckenstein, E. *Langmuir* **1991**, *7*, 2934–2969.

[15] Blankschtein, D.; Puvvada, S. *J. Chem. Phys.* **1990**, *92*, 3710–3724.

[16] Sorensen, T. S. *Acta. Chem. Scand. A* **1982**, *36*, 141–157. *Chem. Eng. Commun.* **1983**, *20*, 93–125.

[17] Diamant, H.; Andelman, D. Models of Gemini Surfactants. In *Gemini Surfactants*; Zana, R.; Xia, J., Eds. Marcel Dekker: New York, 2004; pp 37–64.

[18] Ben-Shaul, A.; Szleifer, I.; Gelbart, W. M. *J. Chem. Phys.* **1985**, *83*, 3597–3611.

[19] Guerin, C. B. E.; Szleifer, I. *Langmuir* **1999**, *15*, 7901–7911.

[20] Dill, K. A.; Flory, P. J. *Proc. Natl. Acad. Sci. USA* **1981**, *78*, 676–680.

[21] Widom, B. *J. Chem. Phys.* **1986**, *84*, 6943–6954.

[22] Smit, B.; Esselink, K.; Hilbers, P. A. J.; Vanos, N. M.; Rupert, L. A. M.; Szleifer, I. *Langmuir* **1993**, *9*, 9–11.

[23] Muller, M.; Schick, M. *Phys. Rev. E* **1998**, *57*, 6973–6978.

[24] Pool, R.; Bolhuis, P. G. *J. Phys. Chem. B* **2005**, *109*, 6650–6657. *Phys. Rev. Lett.* **2006**, *97*, 018302.

[25] Stephenson, B. C.; Beers, K.; Blankschtein, D. *Langmuir* **2006**, *22*, 1500–1513.

[26] Aniansson, E. A. G.; Wall, S. N.; Almgren, M.; Hoffmann, H.; Kielmann, I.; Ulbricht, W.; Zana, R.; Lang, J.; Tondre, C. *J. Phys. Chem.* **1976**, *80*, 905–922.

[27] Aniansson, E. A. G.; Wall, S. N. *J. Phys. Chem.* **1974**, *78*, 1024–1030; **1975**, *79*, 857–858.

[28] Aniansson, E. A. G. *Prog. Colloid Polym. Sci.* **1985**, *70*, 2–5.

[29] De Maeyer, L.; Trachimow, C.; Kaatze, U. *J. Phys. Chem. B* **1998**, *102*, 8024–8028.

[30] Kahlweit, M.; Teubner, M. *Adv. Colloid Interface Sci.* **1980**, *13*, 1–64.

[31] Almgren, M.; Aniansson, E. A. G.; Holmaker, K. *Chem. Phys.* **1977**, *19*, 1–16.

[32] Lessner, E.; Teubner, M.; Kahlweit, M. *J. Phys. Chem.* **1981**, *85*, 1529–1536; **1981**, *85*, 3167–3175.

[33] Hall, D. G. *J. Chem. Soc. Faraday Trans. 2* **1981**, *77*, 1973–2006; **1987**, *83*, 967–983.

[34] Wall, S.; Elvingson, C. *J. Phys. Chem.* **1985**, *89*, 2695–2705.

[35] Kuni, F. M.; Grinin, A. P.; Shchekin, A. K.; Rusanov, A. I. *Colloid J.* **2001**, *63*, 197–204; **2001**, *63*, 723–730.

[36] Nyrkova, I. A.; Semenov, A. N. *Macromol. Theory Simul.* **2005**, *14*, 569–585.

[37] Ball, R.; Haymet, A. D. J. *Phys. Chem. Chem. Phys.* **2001**, *3*, 4753–4761.

[38] Neu, J. C.; Cañizo, J. A.; Bonilla, L. L. *Phys. Rev. E* **2002**, *66*, 061406.

[39] Halperin, A.; Alexander, S. *Macromolecules* **1989**, *22*, 2403–2412.

[40] Haliloglu, T.; Bahar, I.; Erman, B.; Mattice, W. L. *Macromolecules* **1996**, *29*, 4764–4771.

[41] Dormidontova, E. E. *Macromolecules* **1999**, *32*, 7630–7644.

[42] Besseling, N. A. M.; Cohen Stuart, M. A. *J. Chem. Phys.* **1999**, *110*, 5432–5436.

[43] Zana, R.; Marques, C.; Johner, A. *Adv. Colloid Interface Sci.* **2006**, *123–126*, 345–351.

[44] Lund, R.; Willner, L.; Stellbrink, J.; Lindner, P.; Richter, D. *Phys. Rev. Lett.* **2006**, *96*, 068302.

[45] Lund, R.; Willner, L.; Richter, D. *Macromolecules* **2006**, *39*, 4566–4575.

[46] Lund, R.; Willner, L.; Monkenbusch, M.; Panine, P.; Narayanan, T.; Colmenero, J.; Richter, D. *Phys. Rev. Lett.* **2009**, *102*, 188301.

[47] von Gottberg, F.; Smith, K. A.; Hatton, T. A. *J. Chem. Phys.* **1998**, *108*, 2232–2244.

[48] He, X.; Schmid, F. *Phys. Rev. Lett.* **2008**, *100*, 137802.

[49] de Gennes, P.-G.; *Scaling Concepts in Polymer Physics*; Cornell University Press: New York, 1979.

[50] Landau, L. D.; Lifshitz, E. M. *Statistical Physics, Part 1*; 3rd Ed., Butterworth-Heinemann: Oxford, 1980.

[51] Binder, K. *Rep. Prog. Phys.* **1987**, *50*, 783–859.

[52] Gunton, J. G.; Droz, M. *Introduction to the Theory of Metastable and Unstable States, Lecture Notes in Physics Vol. 183*; Springer-Verlag: Berlin, 1983.

[53] Becker, R.; Döring, W. *Ann. der Phys.* **1935**, *24*, 719–752.

[54] Hänggi, P.; Talkner, P.; Borkovec, M. *Rev. Mod. Phys.* **1990**, *62*, 251–341.

[55] Kramers, H. A. *Physica* **1940**, *7* 284–304.

[56] Hadgiivanova, R.; Diamant, H. *J. Phys. Chem. B* **2007**, *111*, 8854–8859.

[57] Woo, H.-J.; Carraro, C.; Chandler, D. *Faraday Discuss.* **1996**, *104*, 183–191. Maibaum, L.; Dinner, A. R.; Chandler, D. *J. Phys. Chem. B* **2004**, *108*, 6778–6781.

[58] Hadgiivanova, R.; Diamant, H. *J. Chem. Phys.* **2009**, *130*, 114901.

[59] Lindman, B.; Brun, B. *J. Colloid Interface Sci.* **1973**, *42*, 388–399.

[60] Sabate, R.; Gallardo, M.; Estelrich, J. *Electrophoresis* **2000**, *21*, 481–485.

[61] Mackie, A. D.; Panagiotopoulos, A. Z.; Szleifer, I. *Langmuir* **1997**, *13*, 5022–5031.

[62] Zettl, H.; Portnoy, Y.; Gottlieb, M.; Krausch, G. *J. Phys. Chem. B* **2005**, *109*, 13397–13401.

[63] Cui, X.; Mao, S.; Liu, M.; Yuan, H.; Du, Y. *Langmuir* **2008**, *24*, 10771–10775.

[64] Jiang, Y.; Chen H.; Cui, X.; Mao, S.; Liu, M.; Luo, P.; Du, Y. *Langmuir* **2008**, *24*, 3118–3121.

[65] Hill, T. L.; *Thermodynamics of Small Systems*; Dover: New York, 1994.

[66] J. S. Langer, Ann. Phys. N. Y. **1969**, *54* 258–275.

[67] Mathias, J. H.; Rosen, M. J.; Davenport, L. *Langmuir* **2001**, *17*, 6148–6154.

[68] Barnadas-Rodriguez, R.; Estelrich, J. *J. Phys. Chem. B* **2009**, *113*, 1972–1982.

[69] Diamant, H.; Andelman, D. *J. Phys. Chem.* **1996**, *100*, 13732–13742.

[70] Diamant, H.; Ariel, G.; Andelman, D. *Colloid Surfaces A* **2001**, *183–185*, 259–276.

[71] Pramauro, E.; Bianco Prevot, A. *Detergent Formulations in Separation Science*; In *Handbook of Detergents, Vol. 128, Part D: Formulation*; Showell, M. S., Ed.; CRC Press: Boca Raton, FL, 2006, Chap. 10, pp. 305–323.

[72] Morigaki, K.; Walde, P.; Misran, M.; Robinson, B. H. *Colloid Surfaces A* **2003**, *213*, 37–44.

[73] Eastoe, J.; Dalton, J. S.; Downer, A. *Langmuir* **1998**, *14*, 1937–1939.

[74] Trachimow, C.; De Maeyer, L.; Kaatze, U. *J. Phys. Chem. B* **1998**, *102*, 4483–4487.